Local hydrogen bonding dynamics and collective reorganization in water: Ultrafast infrared spectroscopy of HOD/D2O

Christopher J. Fecko, Joseph J. Loparo, Sean T. Roberts, and Andrei Tokmakoff

Citation: J. Chem. Phys. **122**, 054506 (2005); doi: 10.1063/1.1839179
View online: http://dx.doi.org/10.1063/1.1839179
View Table of Contents: http://jcp.aip.org/resource/1/JCPSA6/v122/i5
Published by the AIP Publishing LLC.

Local hydrogen bonding dynamics and collective reorganization in water: Ultrafast infrared spectroscopy of HOD/D_2O

Christopher J. Fecko,[a] Joseph J. Loparo, Sean T. Roberts, and Andrei Tokmakoff[b]
Department of Chemistry and George R. Harrison Spectroscopy Laboratory, Massachusetts Institute of Technology, Cambridge, Massachusetts 02139

(Received 26 August 2004; accepted 2 November 2004; published online 18 January 2005)

We present an investigation into hydrogen bonding dynamics and kinetics in water using femtosecond infrared spectroscopy of the OH stretching vibration of HOD in D_2O. Infrared vibrational echo peak shift and polarization-selective pump-probe experiments were performed with mid-IR pulses short enough to capture all relevant dynamical processes. The experiments are self-consistently analyzed with a nonlinear response function expressed in terms of three dynamical parameters for the OH stretching vibration: the frequency correlation function, the lifetime, and the second Legendre polynomial dipole reorientation correlation function. It also accounts for vibrational-relaxation-induced excitation of intermolecular motion that appears as heating. The long time, picosecond behavior is consistent with previous work, but new dynamics are revealed on the sub-200 fs time scale. The frequency correlation function is characterized by a 50 fs decay and 180 fs beat associated with underdamped intermolecular vibrations of hydrogen bonding partners prior to 1.4 ps exponential relaxation. The reorientational correlation function observes a 50 fs librational decay prior to 3 ps diffusive reorientation. Both of these correlation functions compare favorably with the predictions from classical molecular dynamics simulations. The time-dependent behavior can be separated into short and long time scales by the 340 fs correlation time for OH frequency shifts. The fast time scales arise from dynamics that are mainly local: fluctuations in hydrogen bond distances and angles within relatively fixed intermolecular configurations. On time scales longer than the correlation time, dephasing and reorientations reflect collective reorganization of the liquid structure. Since the OH transition frequency and dipole are only weakly sensitive to these collective coordinates, this is a kinetic regime which gives an effective rate for exchange of intermolecular structures. © *2005 American Institute of Physics.* [DOI: 10.1063/1.1839179]

I. INTRODUCTION

Hydrogen bonding has an unusually strong influence on the physical and chemical properties of water, distinguishing it from other liquids. Due to water's low molecular weight, and because each molecule can interact directly with four neighbors, hydrogen bonding allows for the formation of an extended network of molecules. The connectivity of this network is subject to constant fluctuations in local structure and molecular reconfigurations that break and form individual hydrogen bonds. Because these dynamics impact chemical reactions, charge displacement, and biological processes in aqueous solutions, it is essential to understand the physical processes that govern them. Despite many decades of experimental and theoretical investigations of hydrogen bonding in water,[1–6] many mysteries remain about the way hydrogen bonds are made and broken.

Our present understanding of hydrogen bonding dynamics in water comes largely from classical molecular dynamics (MD) computer simulations, typically using models that treat the molecules as rigid bodies with point charges and are parametrized to reproduce thermodynamic data. Simulations have helped describe the time scales for configurational changes in water, from femtosecond fluctuations within relatively fixed intermolecular structures to picosecond cooperative motions of many water molecules as the structure of the liquid rearranges itself. While standard geometric and energetic definitions of a hydrogen bond involve only the local O–H···O configuration of hydrogen bond donor and acceptor, changes to this hydrogen bond involves reconfiguration of the liquid structure, a collective motion that may break and form multiple hydrogen bonds.[2,3]

One persistent difficulty in the experimental study of hydrogen bond dynamics in water is the extremely short characteristic time scales of the relevant molecular motions. Experimental methods, such as x-ray and neutron scattering, are mostly static or time-averaged measures of water's intermolecular structure.[7] Nuclear magnetic resonance (NMR) and dielectric relaxation can measure reorientational correlation times, but are not structurally resolved probes and cannot access sub-picosecond time scales.[8] Time-resolved optical Kerr effect spectroscopy[9–11] and solvation dynamics experiments[5,6,12] can observe these fast processes, but characterize the collective dynamics of many molecules, thereby eliminating sensitivity to local structural changes. New experimental methods that are structurally sensitive to time-

[a]Present address: Applied and Engineering Physics, Cornell University, Ithaca, NY 14853.
[b]Electronic mail: tokmakof@mit.edu

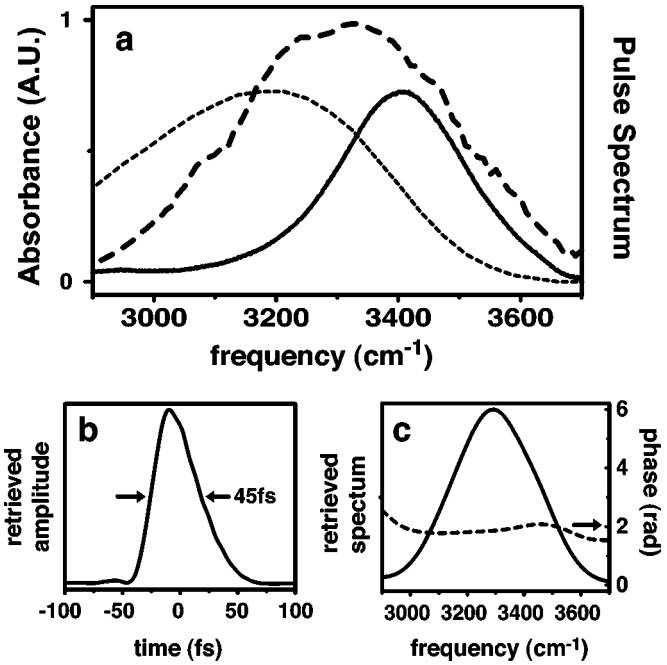

FIG. 1. (a) Linear absorption spectrum of HOD in D_2O in the OH stretching region (solid) and the $|2\rangle \leftarrow |1\rangle$ transition taken from Ref. 22 (dotted) superimposed on the experimental IR pulse spectrum (dash). IR pulse shape (b) and pulse spectrum and phase (c) extracted from a FROG measurement (Ref. 44).

dependent changes in hydrogen bonding configuration in the liquid are needed.

A rapidly evolving method that can potentially structurally resolve changes in hydrogen bonding on femtosecond and picosecond time scales and make direct contact to MD simulations is time-resolved infrared spectroscopy.[13] This approach has long been used to study the motions of water molecules because the vibrational frequency of an OH oscillator depends strongly on its local environment. Experiments on crystals containing O–H···O hydrogen bonds have correlated the OH stretching vibrational frequency ω with the hydrogen bond length, R_{OO}.[14] Because of the distribution of rapidly changing hydrogen bonding configurations that exists within the liquid state, the linear OH absorption spectrum is extremely broad (Fig. 1). Although broadening hides dynamic information in the IR spectrum, femtosecond time-resolved infrared spectroscopy can characterize time-dependent OH frequency fluctuations and spectral diffusion, and thereby infer changes in the configuration of solvent molecules around the oscillator. The quantitative measure of these frequency fluctuations is the OH frequency correlation function:

$$C(t) = \langle \delta\omega(t)\,\delta\omega(0)\rangle, \tag{1}$$

where $\delta\omega(t)$ is the difference between $\omega(t)$ and its time-averaged value. We refer to the vibrational dynamics of the OH stretch frequency fluctuations and spectral diffusion characterized by $C(t)$ as vibrational dephasing.

The development of time-resolved IR experiments on water has recently been reviewed.[13] The most common system to study hydrogen bond dynamics in water is the OH stretching vibration of HOD in D_2O. By eliminating the intermolecular OH vibrational couplings, the dynamics of a localized OH vibration can be observed isolated amongst D_2O molecules whose hydrogen bonding dynamics closely resemble that of H_2O. Vibrational dephasing, as well as energy relaxation and molecular reorientations, have been investigated with transient hole-burning (THB) experiments, in which a narrow-band IR pump laser excites a nonequilibrium distribution of OH vibrations, and a second IR probe pulse follows the time-dependent relaxation to equilibrium.[15–26] Although there is some discrepancy between the results and interpretations from different groups, these studies have found spectral relaxation on time scales of 0.5–1 ps. This relaxation process has been attributed to diffusive changes in R_{OO}, hydrogen bond making and breaking, and changes in tetrahedrality or coordination number about the HOD.[17,22,25] OH vibrational population relaxation from the first excited state is reported to occur in 500–1000 fs,[15,17,18,23–25,27] and individual molecules undergo reorientational motion on a 3 ps time scale in the ground state.[17,21] The inherent tradeoff between time and frequency resolution in THB experiments has limited their observations to time scales >200 fs. More recently, vibrational dephasing has been investigated with techniques based on IR vibrational echoes, finding additional decay components of 30–130 fs.[28–33] These studies are pushing into the short time regime associated with intermolecular structural fluctuations in water, allowing direct connections to a number of recent theoretical studies on OH vibrational dephasing that draw on MD simulations. In particular, it is predicted that underdamped intermolecular oscillations between hydrogen bonding partners should be observed on ~ 160 fs time scales prior to the configurational changes that accompany hydrogen bond breaking.[31,34–38]

Up to this point a comprehensive description of the vibrational dynamics of HOD in D_2O has not emerged. This is partially because previous studies have used pulses whose Fourier-transform limited bandwidth is narrower than the absorption line shape, ensuring that faster line-broadening dynamics are being missed. It is also due to the complications in accounting for vibrational dephasing, population decay, and molecular reorientation, which all contribute to experimental observables on similar time scales. (We refer to the combined effect of these three processes generically as vibrational dynamics, due to their influence on the IR spectroscopy.) Additionally, recent studies have highlighted the importance of modeling spectral shifts due to the excess energy transferred to intermolecular motion upon OH vibrational relaxation.[29,30,39] These longer time thermalization effects are important to include in modeling vibrational dynamics on picosecond time scales.

In this paper we dissect the OH vibrational dynamics of HOD in D_2O, using a unified analysis of multiple selective femtosecond infrared experiments, which are performed with mid-IR pulses short enough to resolve all of the processes that broaden the OH vibrational line shape. The modeling is based on correlation functions, which offers an ensemble average perspective of the vibrational dynamics, and allows direct comparison to molecular dynamics simulations. This work expands on our recent brief reports of ultrafast infrared

experiments on HOD/D_2O and comparison to modeling based on MD simulations.[31,32]

We present polarization-selective broadband pump-probe (PP) and three-pulse vibrational echo peak shift (PS) spectroscopies used to observe population relaxation and dephasing of OH oscillators, as well as molecular reorientations. PP experiments measure pump-induced transmission changes of a weak probe beam as a function of the time delay, and are primarily sensitive to vibrational population relaxation and molecular reorientations. Experiments with varying light field polarization allow the separation of these two contributions. The PS measurements are most sensitive to the time scales of vibrational dephasing. In this experiment, a periodic frequency grating arising from a short pulse pair separated by a delay τ_1 is used to excite the OH stretching line shape. During a waiting time τ_2, this frequency grating is gradually erased due to the spectral diffusion processes accompanying hydrogen bonding reconfigurations, after which a third pulse is scattered off any residual grating. The PS measurement determines the value of τ_1 that maximizes the integrated scattered signal τ_1^* as a function of τ_2. The PS decay with τ_2 is directly related to the frequency correlation function for the system $C(t)$ and has been applied to a variety of electronic[40,41] and vibrational[31,42,43] systems.

Following the experiments, we develop a unified description of the OH vibrational dynamics of HOD in D_2O by analyzing the PP and PS results using a nonlinear response function that incorporates all of the relaxation processes. Our experiments can be self-consistently reconstructed from three dynamical quantities that describe vibrational dephasing, vibrational population lifetime, and molecular reorientation. Aside from these, our model requires only three static quantities that describe the center frequencies of the fundamental and overtone transitions, as well as the OH frequency shift that results from relaxation-induced heating of the surroundings. By treating the data in this way, each resulting dynamical quantity is free from the influences of the others for the entire range of the experiments, from tens of femtoseconds to several picoseconds.

We conclude with a comparison with previous experimental and theoretical work, and make direct comparison of our results to predictions of vibrational dephasing and molecular reorientation from classical MD simulations. The results indicate that the vibrational dynamics can be separated into two time regimes by the 340 fs correlation time for $C(t)$. The shortest time scales reflect a dynamic regime, in which transient IR experiments are sensitive to configurational fluctuations within local hydrogen bonding environments. The longer, picosecond time scales are characterized by exponential relaxation that arises from the collective reorganization of the structure of water. IR experiments of the OH stretch are only weakly sensitive to the many-body reconfigurations in this kinetic regime, and the relaxation measures rates for exchange of different hydrogen bonding structures.

II. EXPERIMENTS

A home-built optical parametric amplifier (OPA) pumped by a Ti:sapphire laser system generated the ultrashort mid-IR pulses required for the nonlinear experiments presented here. A detailed description of the OPA and mid-IR pulse characteristics is presented elsewhere.[44] Briefly, 800 nm, sub-30 fs pulses from a 1 kHz repetition rate multipass Ti:sapphire amplifier pump a white-light seeded two-stage OPA design to produce the 3 μm pulses. In this scheme, the initial 1.1 μm seed is derived from continuum generated in sapphire, parametrically amplified in the first stage using a 1 mm β-barium borate crystal, and subsequently mixed with 800 nm in a 1 mm potassium niobate crystal to generate 3–4 μJ pulse energies in the 3 μm wavelength range. We characterize the mid-IR pulses in frequency by recording their spectrum, and in time by second-order background-free autocorrelation or frequency-resolved optically gating (FROG).[45] A characterization provided in Fig. 1 shows that the coherent bandwidth is typically 350 cm^{-1}, with a relatively flat spectral phase. This bandwidth is larger than the OH absorption linewidth, ensuring that all dynamical processes that broaden the OH line can be observed in the spectroscopic measurements. The time duration of the retrieved field was 52 fs for the PS measurements presented here and 45 fs for the pump-probe measurements.

The IR beam is expanded in a Galilean telescope using CaF_2 lenses spaced to collimate the beam to a diameter of 8 mm, which allows propagation for several meters without significant divergence. To simplify subsequent alignment, the IR beam is overlapped with a mode-matched HeNe beam using a 2 mm thick Ge window. The Ge window also aids in IR pulse compression, which is achieved by adjusting the total amount of group velocity dispersion (GVD) imparted by the materials in the beam path to minimize the pulse duration at the sample.[44,46] Each pulse is split into three replicas of itself in a modified Mach-Zender interferometer similar to those described previously.[47] This interferometer employs custom 3 μm 50/50 CaF_2 beam splitters designed to minimize the GVD of the transmitted and reflected beams (Thin Film Laboratory). Each arm contains the appropriate number of CaF_2 compensation plates to balance the total amount of material traversed by the beam and a 3 mm thick CaF_2 wire grid polarizer (Optometrics) to control the polarization. Retroreflectors mounted on computer controlled translation stages (Aerotech ANT25-L) vary the relative delay between pulses derived from each arm. Beams are focused into the sample by a 100 mm effective focal length, off-axis parabolic mirror (Janos) to a spot size ($2w$) of 100 μm.

The experimental setup for vibrational PS experiments is similar to those described for the analogous electronic experiments.[40,41] Three of the beams exiting the interferometer are arranged in an equilateral triangle geometry with parallel polarizations. Liquid nitrogen cooled InSb detectors record the integrated echo signal simultaneously in the two phase-matched directions $\mathbf{k}_- = -\mathbf{k}_\alpha + \mathbf{k}_\beta + \mathbf{k}_\gamma$ and $\mathbf{k}_+ = +\mathbf{k}_\alpha - \mathbf{k}_\beta + \mathbf{k}_\gamma$, where the subscripts α, β, and γ label the incident beams but do not necessarily indicate the relative time orderings. A 500 Hz mechanical chopper placed in one

arm of the interferometer blocks every other pulse, and the detector signals are acquired with lock-in detection. The integrated echoes are recorded as a function of the delay between pulses α and β, τ_1, for fixed values of the waiting time τ_2. Because echoes in the $\mathbf{k}_+$ and $\mathbf{k}_-$ directions are equivalent under exchange of the α and β indices, their time profiles are symmetric about $\tau_1=0$. The peak shift is half of the time period between the two maxima, which reduces the influence of errors on the determination of τ_1^* due to inexact knowledge of pulse timings. We measure a FROG immediately following each PS data set to account for the pulse amplitude and phase characteristics in calculations to extract the correlation function.

To record the PP decay, a mechanical chopper is placed in one of the three beams, which acts as the pump. After the sample, the pump beam is blocked and the remaining two beams (which act as probe and reference) both pass through a bandpass filter (Spectragon) centered at 3400 cm^{-1} (see Fig. 3) to record the time-dependent PP decay. The InSb detectors measure the intensity of each beam, and the laser noise is partially removed by normalizing the PP signal by the intensity of the reference beam I_R: $S_{PP}(\tau)=\ln(I'_{pr}/I_R)-\ln(I_{pr}/I_R)$, where I'_{pr} (I_{pr}) is the intensity of the probe beam in the presence (absence) of the pump beam. In this notation, an induced absorption is negative and a bleach is positive. The polarization of the pump and probe are varied independently, and the probe beam passes through an analyzing wire-grid polarizer after the sample. Because waveplates are not included in our interferometer, energy balanced PP decays needed to calculate the anisotropy were recorded by rotating the polarizer in the probe arm of the interferometer to 45° with respect to the pump polarization, then rotating the analyzing polarizer to 0° or 90°. The relative scaling of the PP signals for different polarization conditions were checked carefully by averaging the $\tau=0$ signal.

The sample, a $\sim$1% solution of HOD in D_2O, is flowed continuously as a 50 μm path length jet. The concentration was adjusted to produce a peak optical density (OD) in the range of 0.3–0.4 at the outset of the experiment, and was tested at the end of each data set to ensure that the change in OD did not exceed 0.05. By using a free-flowing jet instead of a sample cell, we avoid any signal contribution from the sample cell walls that obscure features in the HOD signals for times up to 250 fs.

III. RESULTS

Typical experimentally measured integrated echoes are plotted in Fig. 2 for several waiting times. Peak shift values were determined by fitting both integrated echo profiles with Gaussian functions for times within 50 fs of the maximum signal. The PS signal resulting from this fit (Fig. 2) decays from an initial value of $\tau_1^*=28$ fs with characteristic time scales of 75 fs and 1.2 ps, but exhibits a weak recurrence that peaks at 150 fs. As we have noted previously, the amplitudes and time scales of the short time features depend on the pulse characteristics, but the differences are reproduced by including the experimentally determined pulse characteristics in the numerical calculations.[31] As other studies have noted, the

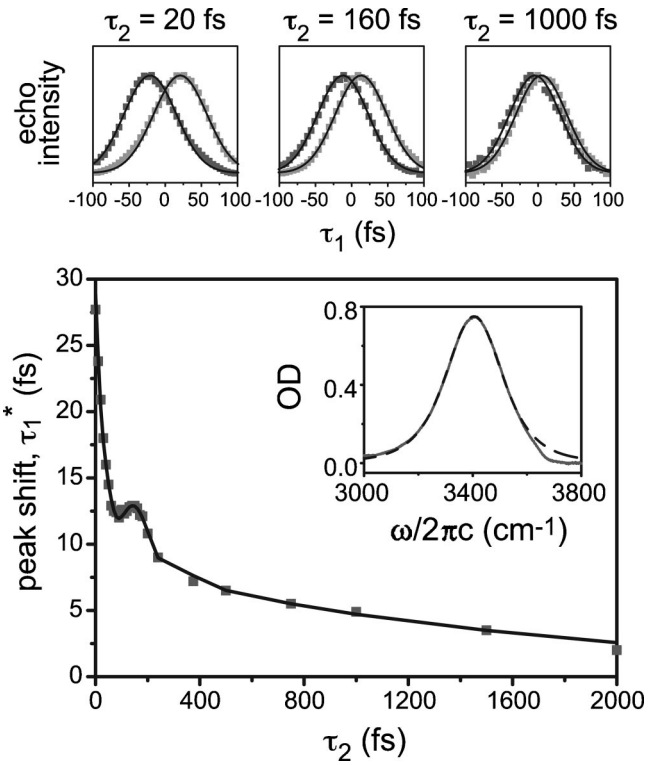

FIG. 2. Top: Examples of normalized vibrational echoes in the $\mathbf{k}_+$ and $\mathbf{k}_-$ wave vector geometries for the indicated waiting times. For each τ_2, the value of τ_1^* is obtained by fitting both echoes with Gaussian functions (black lines) to determine the time interval between peak positions. Bottom: The PS decay (squares) is plotted along with the best fit (black line). In the inset, the absorption spectrum calculated from the extracted dynamical quantities (dashed line) is superimposed on the experimental spectrum.

integrated echoes exhibit a slight asymmetry at waiting times less than the pulse duration ($\tau_2<50$ fs), causing the peak of the signal to deviate slightly from the center of the Gaussian fit.[48] The asymmetry is largely reproduced in the calculations to extract $C(t)$ discussed below.

We also measured a set of frequency-dispersed PS (Fig. 3) by inserting bandpass filters directly after the sample, so that the echo signals in both phase matching directions were spectrally filtered. The center frequencies of the filters spanned the fundamental and $v=1\rightarrow2$ transition frequencies. The dispersed PS decays differ in their initial value, which is as small as 16 fs for the filter centered at 3500 cm^{-1} and as large as 44 fs for the 3160 cm^{-1} filter. However, each of the curves reach a value of $\tau_1^*=10-14$ fs by $\tau_2=100$ fs and show a clear sign of a recurrence that peaks in the range of 120–180 fs.

The time-dependent PP decay at 3400 cm^{-1} is plotted in Fig. 4, which includes signals for experiments in which the polarizer in the pump beam is oriented parallel (0°, S_{ZZZZ}), perpendicular (90°, S_{ZZYY}), or at the magic angle (54.7°, S_{ZZMM}) with respect to the polarizers along the probe beam. All three signals contain nonexponential behavior at short pulse delay times ($\tau_2>400$ fs), single-exponential or biexponential behavior for intermediate times (400 fs$<\tau_2<4$ ps), and a 3.5% offset (see Fig. 5) that remains constant to at least $\tau_2=50$ ps. Of these, the intermediate time scale

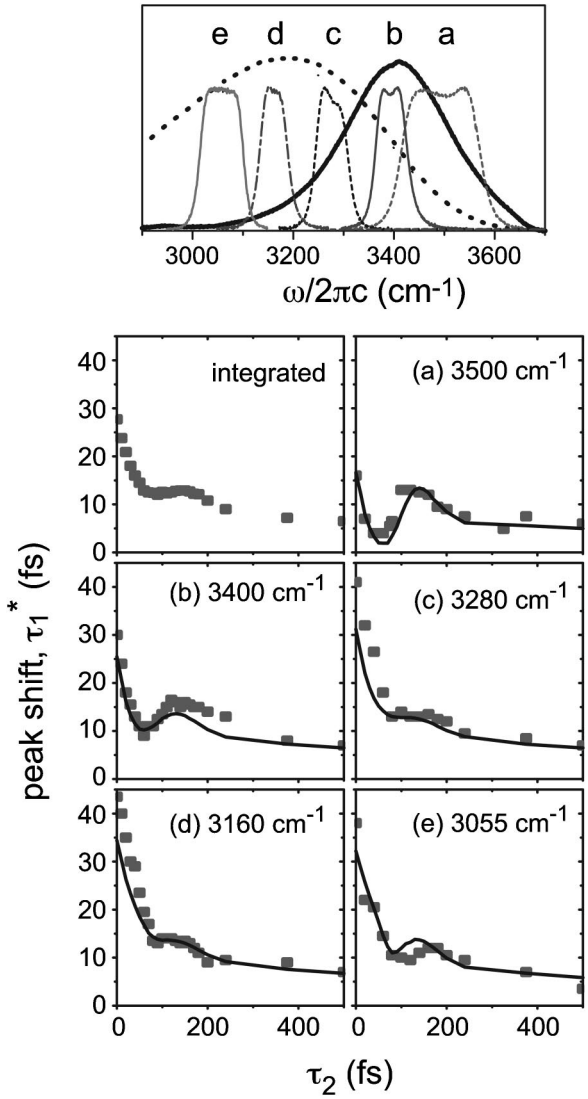

FIG. 3. (Top) Transmission spectra of the bandpass filters used to collect the PP and dispersed PS superimposed on the OH fundamental (solid black) and projected overtone (Ref. 22) (dotted black) spectra. (a) 3500 cm^{-1}, (b) 3400 cm^{-1}, (c) 3280 cm^{-1}, (d) 3160 cm^{-1}, (e) 3055 cm^{-1}. (Bottom) Experimentally measured dispersed PS decays of HOD in D_2O (squares) and predicted dispersed PS signals using dynamical quantities extracted from the frequency-integrated measurements.

contains the most useful information, namely, the dynamics of vibrational population relaxation and molecular reorientation. The intermediate decay times of the three polarization conditions, highlighted by a semilog plot of the normalized signals from which the long time offset has been removed by subtraction (Fig. 4), differ in the contribution to each from molecular reorientations. The magic angle signal (MA-PP), which is free from the effects of reorientations,[49] exhibits a single exponential decay at long times ($\tau_2 > 400$ fs), indicating a OH population lifetime of $T_1 = 700$ fs. To determine the effects of reorientations, the time-dependent anisotropy $r(t)$ (Fig. 6) was calculated from the parallel and perpendicular experimental signals as

$$r(\tau_2) = \frac{S_{ZZZZ}(\tau_2) - S_{ZZYY}(\tau_2)}{S_{ZZZZ}(\tau_2) + 2S_{ZZYY}(\tau_2)}. \quad (2)$$

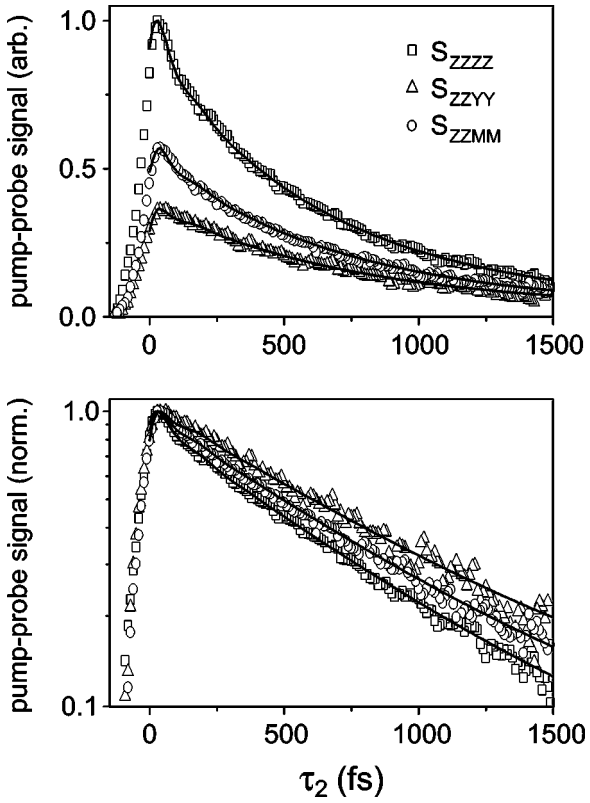

FIG. 4. Pump-probe signals in parallel (S_{ZZZZ}, squares), perpendicular (S_{ZZYY}, triangles), and magic angle geometries (S_{ZZMM}, circles). The bottom panel is a semilog plot of the normalized signals obtained after subtracting the asymptotic offset to highlight the relative decay rates.

Its initial value $r(0)$ is 0.38, approaching the limiting value of 0.4 and indicating that our measurement captures nearly all of the molecular reorientational dynamics. The raw data is fit well by a biexponential function with decay time constants of 60 and 3000 fs.

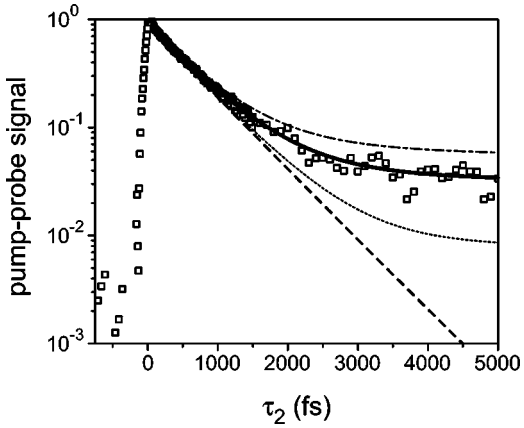

FIG. 5. Experimentally measured parallel pump-probe, which decays to a 3.5% offset. Lines show calculated pump-probe signals using the extracted dynamical quantities and varying HGS parameters $\Delta\omega$ and $\Delta\mu$ that reflect the change in frequency and transition moment. The dashed line shows the exponential lifetime decay with a rate of 700 fs ($\Delta\omega = 0$ and $\Delta\mu = 0$). The solid line is the best fit signal with $\Delta\omega = 12$ cm^{-1} and $\Delta\mu = 0.05$. Also shown are $\Delta\omega = 20$ cm^{-1}, $\Delta\mu = 0$ (dotted); and $\Delta\omega = 20$ cm^{-1}, $\Delta\mu = 0.08$ (dash-dot).

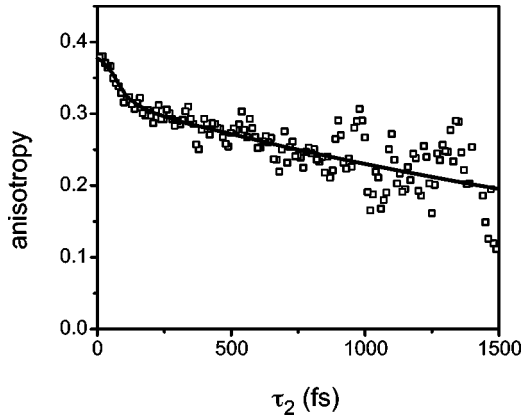

FIG. 6. Anisotropy decay $r(\tau_2)$ determined from the parallel and perpendicular pump-probe signals. The line is the anisotropy calculated from the extracted dynamical quantities and pulse shape.

IV. SELF-CONSISTENT DATA MODELING

A. Response function formalism

In order to separate contributions to the OH vibrational spectroscopy, we have fit the experimental PS and PP data by numerically convoluting the input fields with a response function that accounts for dephasing, lifetime, and reorientation, as well as the thermalization effects present in the data. Our model is derived from the work of Sung and Silbey, who derived a theory for four wave mixing (FWM) experiments of a multilevel system coupled to a bath with arbitrary time scales.[50,51] The model is based on a Hamiltonian that is partitioned into terms for the molecular degrees of freedom and their interactions with the incident IR pulses: $H=H_0+H_{\mathrm{int}}$. H_0 is further divided into the system Hamiltonian for the OH stretch vibration which couples to the external fields, the bath Hamiltonian for the remaining intramolecular and intermolecular degrees of freedom, and the system-bath interaction: $H_0=H_S+H_B+H_{\mathrm{SB}}$. In our case, H_S is an anharmonic oscillator with system eigenstates $\upsilon=0$, 1, and 2,

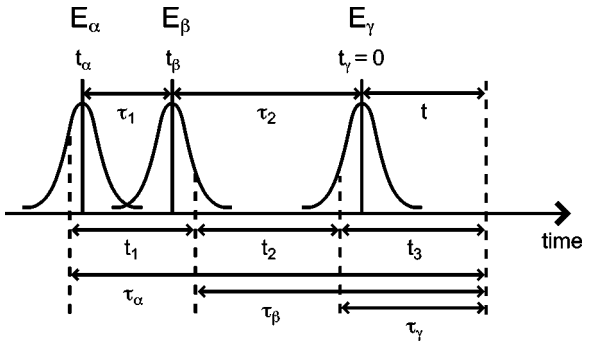

FIG. 7. Illustration of the time variables used in calculating the nonlinear polarization. Time flows from left to right. t_α, t_β, and t_γ are the times at which the center of each pulse arrives at the sample. The polarization is calculated a time t after the third pulse. t_γ is defined as the time origin so that t_α and t_β are both negative and t is positive as shown. The pulse delay times are defined by $\tau_1=t_\beta-t_\alpha$ and $\tau_2=t_\gamma-\max(t_\beta,t_\alpha)$. Dashed vertical lines indicate interaction times within each pulse, which occur at the positive valued times τ_α, τ_β, and τ_γ before the point t. t_1, t_2, and t_3 are the positive valued time periods between the interactions and are always numbered consecutively, regardless of pulse ordering.

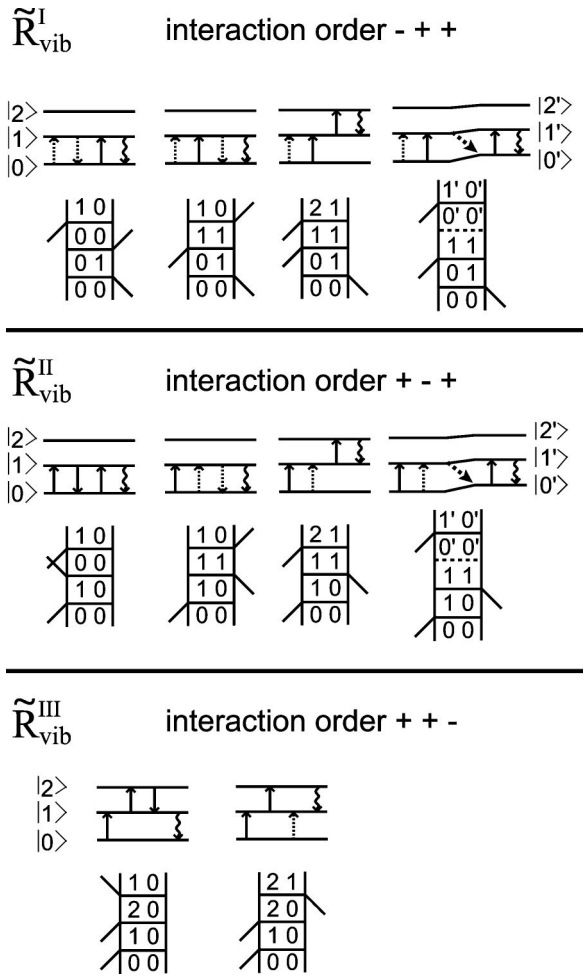

FIG. 8. Feynman and associated ladder diagrams representing the evolution of the density matrix for terms that survive the RWA for a three level system in the phase-matching direction $\mathbf{k}_{\mathrm{sig}}=-\mathbf{k}_\alpha+\mathbf{k}_\beta+\mathbf{k}_\gamma$. Each row lists one of the contributing responses $\tilde{R}^{\mathrm{I}}_{\mathrm{vib}}$, $\tilde{R}^{\mathrm{II}}_{\mathrm{vib}}$ and $\tilde{R}^{\mathrm{III}}_{\mathrm{vib}}$ which contribute only when the time-ordered interactions satisfies the conditions listed. The final diagrams for $\tilde{R}^{\mathrm{I}}_{\mathrm{vib}}$ and $\tilde{R}^{\mathrm{II}}_{\mathrm{vib}}$ account for the HGS. The dashed horizontal lines in the Feynman diagrams and thick dashed arrows in the ladder diagrams indicate population relaxation during the second time period.

where the fundamental ($|1\rangle\leftarrow|0\rangle$) energy difference is ω_{10} and the $|2\rangle\leftarrow|1\rangle$ transition $\omega_{21}=\omega_{10}-\Delta$ is redshifted by the anharmonicity Δ.

In a FWM experiment, three input electromagnetic fields create a macroscopic polarization within the sample, which subsequently radiates a fourth, signal field. By perturbatively expanding the material polarization in terms of the incident fields, the third-order polarization $\mathbf{P}^{(3)}$ can be expressed as triple convolution of a response function $\mathbf{R}$ with the incident fields $\mathbf{E}$:[52]

$$\mathbf{P}^{(3)}(t)=\int_0^\infty dt_3\int_0^\infty dt_2\int_0^\infty dt_1\mathbf{R}(t_3,t_2,t_1)\mathbf{E}(t-t_3)\times\mathbf{E}(t-t_3-t_2)\mathbf{E}(t-t_3-t_2-t_1). \quad (3)$$

t_1 and t_2 are the positive valued time periods that separate the three field-matter interactions and t_3 is the time between the last interaction and detection of the polarization at time t (Fig. 7). The tensorial response function is a thrice-nested

commutator of the transition dipole operator $\boldsymbol{\mu}$ evaluated at times corresponding to each field-matter interaction:

$$\mathbf{R}(t_3,t_2,t_1)=\left(\frac{i}{\hbar}\right)^3\langle[[\boldsymbol{\mu}(t_3+t_2+t_1),\boldsymbol{\mu}(t_2+t_1)],\boldsymbol{\mu}(t_1)],\boldsymbol{\mu}(0)]\rangle. \tag{4}$$

Because the dipole operator evolves according to H_0, the response function contains information about the microscopic dynamics of the sample. This response function can be cast in terms of $C(t)$ by using the second cumulant approximation, which is valid for the case that the frequency fluctuations follow Gaussian statistics.[53]

Our experiments are performed with pulses of light that have a finite duration, and well-defined polarization and wave vectors. To account for these characteristics, the electric field is expressed in terms of three incident pulses:

$$\mathbf{E}(t)=\sum_{\chi=\alpha,\beta,\gamma}\tilde{E}_J(\mathbf{k}_\chi,t_\chi,t)+\text{c.c.}, \tag{5}$$

$$\tilde{E}_J(\mathbf{k}_\chi,t_\chi;t)=\frac{1}{2}\hat{\mathbf{J}}\tilde{e}(t-t_\chi)\exp\{i[\mathbf{k}_\chi\cdot\mathbf{r}-\omega_\chi(t-t_\chi)]\}, \tag{6}$$

where the χth pulse is polarized in the $\hat{\mathbf{J}}$ direction and propagates with wave vector $\mathbf{k}_\chi$. The frequency ω_χ is near resonance with ω_{10} and ω_{21}. The envelope function $\tilde{e}(t-t_\chi)$ can incorporate idealized or experimentally measured amplitude and phase variations.[54] The vibrational echo or pump-probe signal field is radiated in the phase-matched direction $\mathbf{k}_{\text{sig}}=-\mathbf{k}_\alpha+\mathbf{k}_\beta+\mathbf{k}_\gamma$. We apply the rotating wave approximation (RWA), retaining only those terms in the response function that are approximately resonant with the electric field terms.[53] Feynman diagrams representing the evolution of the density matrix for terms that survive the RWA are plotted in Fig. 8. Note that the order in which pulses with positive and negative wave vector components interact with the sample determines the specific terms that contribute to the response function. The polarization resulting from the RWA, written in terms of pulse-labeled interaction times to simplify the notation (see Fig. 7) is

$$\begin{aligned}P^{(3)}_{IJKL}(\mathbf{k}_{\text{sig}},t_\beta,t_\alpha;t)&=\int_0^\infty d\tau_\gamma\int_0^\infty d\tau_\beta\int_0^\infty d\tau_\alpha\tilde{R}_{\text{vib}}(\tau_\gamma,\tau_\beta,\tau_\alpha)\\&\times Y_{IJ'K'L'}(\tau_\gamma,\tau_\beta,\tau_\alpha)\tilde{E}_J(\mathbf{k}_\gamma,t_\gamma\equiv 0;t-\tau_\gamma)\\&\times\tilde{E}_K(\mathbf{k}_\beta,t_\beta;t-\tau_\beta)\tilde{E}_L(\mathbf{k}_\alpha,t_\alpha;t-\tau_\alpha)+\text{c.c.}\end{aligned} \tag{7}$$

The subscripts I, J, K, L (and their primed counterparts) are indices for unit vectors in the laboratory frame (X,Y,Z). In Eq. (7), we have decomposed the response function into a product of vibrational $\tilde{R}_{\text{vib}}$ and orientational Y_{IJKL} contributions. This separation is exact when H_S is factorable into vibrational and rotational terms (with no cross terms between the two). The form of the response function depends on the pulse interaction order:

$$\tilde{R}_{\text{vib}}(\tau_\gamma,\tau_\beta,\tau_\alpha)Y_{IJ'K'L'}(\tau_\gamma,\tau_\beta,\tau_\alpha)=\begin{cases}\tilde{R}^{\text{I}}_{\text{vib}}(\tau_\gamma,\tau_\beta-\tau_\gamma,\tau_\alpha-\tau_\beta)Y_{IJKL}(\tau_\gamma,\tau_\beta-\tau_\gamma,\tau_\alpha-\tau_\beta), & \tau_\alpha>\tau_\beta\geqslant\tau_\gamma\\ \tilde{R}^{\text{I}}_{\text{vib}}(\tau_\beta,\tau_\gamma-\tau_\beta,\tau_\alpha-\tau_\gamma)Y_{IKJL}(\tau_\beta,\tau_\gamma-\tau_\beta,\tau_\alpha-\tau_\gamma), & \tau_\alpha\geqslant\tau_\gamma>\tau_\beta\\ \tilde{R}^{\text{II}}_{\text{vib}}(\tau_\gamma,\tau_\alpha-\tau_\gamma,\tau_\beta-\tau_\alpha)Y_{IJLK}(\tau_\gamma,\tau_\alpha-\tau_\gamma,\tau_\beta-\tau_\alpha), & \tau_\beta\geqslant\tau_\alpha\geqslant\tau_\gamma\\ \tilde{R}^{\text{II}}_{\text{vib}}(\tau_\beta,\tau_\alpha-\tau_\beta,\tau_\gamma-\tau_\alpha)Y_{IKLJ}(\tau_\beta,\tau_\alpha-\tau_\beta,\tau_\gamma-\tau_\alpha), & \tau_\gamma>\tau_\alpha\geqslant\tau_\beta\\ \tilde{R}^{\text{III}}_{\text{vib}}(\tau_\alpha,\tau_\gamma-\tau_\alpha,\tau_\beta-\tau_\gamma)Y_{ILJK}(\tau_\alpha,\tau_\gamma-\tau_\alpha,\tau_\beta-\tau_\gamma), & \tau_\beta>\tau_\gamma>\tau_\alpha\\ \tilde{R}^{\text{III}}_{\text{vib}}(\tau_\alpha,\tau_\beta-\tau_\alpha,\tau_\gamma-\tau_\beta)Y_{ILKJ}(\tau_\alpha,\tau_\beta-\tau_\alpha,\tau_\gamma-\tau_\beta), & \tau_\gamma\geqslant\tau_\beta>\tau_\alpha.\end{cases} \tag{8}$$

The vibrational response functions $\tilde{R}^{\text{I}}_{\text{vib}}$, $\tilde{R}^{\text{II}}_{\text{vib}}$ and $\tilde{R}^{\text{III}}_{\text{vib}}$ are the sum of all density matrix pathways that contribute within the RWA for a given interaction ordering (Fig. 8). They differ from the well-known nonlinear response functions for electronic spectroscopy because they include terms that depend on the overtone transition. The existence of $\tilde{R}^{\text{III}}_{\text{vib}}$ is unique to a multilevel system, where it is possible to have a coherence between the $|0\rangle$ and $|2\rangle$ eigenstates during t_2. These pathways only contribute to the experiments simulated here when the pulses overlap. The $\tilde{R}^{\text{I}}_{\text{vib}}$ pathways are rephasing, with oscillation frequencies during the third time period (t_3) that are conjugate or nearly conjugate to those during the first time period (t_1). $\tilde{R}^{\text{II}}_{\text{vib}}$ and $\tilde{R}^{\text{III}}_{\text{vib}}$ are nonrephasing because they oscillate with the same frequency during both time periods.[47] The rephasing character of the density matrix for $\tilde{R}^{\text{I}}_{\text{vib}}$ relies on the frequency correlation during t_1 and t_3, which is diminished and eventually lost as the time between the second and third interactions t_2 is increased. This memory loss is the basis for the vibrational PS experiments.

Within the Condon approximation that sets transition dipole moments to a constant value, Sung and Silbey derived analytical expressions for vibrational dephasing of each pathway in terms of nonlinear dephasing functions $F^{(n)}_{abcd}$ $(a,b,c,d\in 0,1,2,\ldots)$.[50] Using the second cumulant approximation, the dephasing functions are expressed in terms of two-point energy gap correlation functions between the system eigenstates:

$$C_{ab}(\tau-\tau')=\langle\delta\omega_{a0}(\tau)\,\delta\omega_{b0}(\tau')\rangle_B. \tag{9}$$

Analytical expressions for the dephasing functions in terms

TABLE I. Nonvanishing tensor components for the orientational contribution of the response function Y for parallel transition moments written in terms of the first and second Legendre polynomials $p_\ell(t)$ for the unit dipole correlation function. The magic angle (or isotropic) signal is $Y_{ZZMM} \equiv Y_{ZZZZ}+2Y_{ZZYY}$.

Designation	Tensor element	Orientational response
Parallel	$Y_{ZZZZ}(t_3,t_2,t_1)$	$\frac{1}{9}p_1(t_1)[1+\frac{4}{5}p_2(t_2)]p_1(t_3)$
Perpendicular	$Y_{ZZYY}(t_3,t_2,t_1)$	$\frac{1}{9}p_1(t_1)[1-\frac{2}{5}p_2(t_2)]p_1(t_3)$
Anisotropic	$Y_{ZYZY}(t_3,t_2,t_1)$ $=Y_{ZYYZ}(t_3,t_2,t_1)$	$\frac{1}{15}p_1(t_1)p_2(t_2)p_1(t_3)$

of $C(t)$ are given in the Appendix. Here and below we reduce the number of variables in the model by using harmonic scaling relations to relate the vibrational dynamics of various transitions involving $\upsilon=0$, 1, and 2.[47] For the energy gap fluctuations between the three states

$$C_{22}(t)=2C_{21}(t)=2C_{12}(t)=4C_{11}(t)\equiv 4C(t), \tag{10}$$

where $C(t)$ describes all frequency fluctuations of the system.

The orientational response tensor Y_{IJKL} takes into account the effect of molecular reorientation on the nonlinear signal by sequentially projecting the electric field polarizations in the laboratory coordinates onto the distribution of molecular coordinates at the time of each field-matter interaction. Each of these can be written in terms of the reorientational correlation functions of the transition dipole unit vectors $\hat{\mu}$,

$$p_\ell(t)=\langle P_\ell[\hat{\mu}(t)\cdot\hat{\mu}(0)]\rangle, \tag{11}$$

where P_ℓ is the ℓth-order Legendre polynomial. For our model, we apply analytical expressions for Y_{IJKL} derived for spherical rotors (Table I),[49] with the implicit assumption that all transition moments lie along the same molecular axis $(\hat{\mu}_{10}||\hat{\mu}_{21})$. The rotational correlation functions for the case of isotropic orientational diffusion can be written in terms of an orientational diffusion constant D_{or}: $p_\ell(t)=\exp[-\ell(\ell+1)D_{\mathrm{or}}t]$. For the purposes of casting reorientational motion in our model in terms of one observable, we draw on this expression for the diffusive scaling relationship $p_1(t)=p_2(t/3)$.

To account for the effects of population relaxation on the experimental signals, we introduce phenomenological exponential relaxation rates into $\tilde{R}_{\mathrm{vib}}$ during all three time periods. Our rates differ somewhat from analogous approaches used previously in modeling vibrational echoes.[42] For the density matrix element ρ_{ab}, Γ_{ab} is the Markovian relaxation rate neglecting any effects of pure dephasing.[53] Given the relaxation rates for populations in the system states Γ_{aa}, their influence on the relaxation of coherences is an average over the two states of the superposition $\Gamma_{ab}=1/2(\Gamma_{aa}+\Gamma_{bb})$.[55] For a harmonic multilevel vibrational system with linear coupling to the bath, the population relaxation scales with the quantum number, i.e., $\Gamma_{aa}=a\Gamma_{11}$.[56] Using these relationships, we can express the vibrational energy relaxation for all populations and coherences sampled in our experiments by a single quantity, the vibrational lifetime of the first excited vibrational state of the OH stretch, $T_1=1/\Gamma_{11}$:

$$\Gamma_{11}(t)=\tfrac{1}{2}\Gamma_{22}(t)=\Gamma_{10}(t)=\tfrac{2}{3}\Gamma_{21}(t)=\tfrac{2}{3}\Gamma_{20}(t). \tag{12}$$

In the conventional picture, vibrational relaxation of molecules excited by a laser pulse results in the repopulation of the ground state, treating the solvent as a bath that absorbs the excess energy without change. However, previous experiments show that excited state relaxation on the time scale of T_1 leads to excitation of low-frequency intermolecular motions that appears as a nonthermal population of bath states.[29,30,33] To model the effect of this thermalization process on our nonlinear signal, we take an approach similar to the hot ground state (HGS) model of Stenger and co-workers.[29] This response function includes an additional term in each of $\tilde{R}^{\mathrm{I}}_{\mathrm{vib}}$ and $\tilde{R}^{\mathrm{II}}_{\mathrm{vib}}$ that accounts for the changes in the characteristics of the system eigenstates due to a change of occupation in the bath states. These terms add an additional absorption from the thermalized or "hot" ground state during t_3 (Fig. 8), which increase in amplitude during t_2 as molecules undergo vibrational relaxation.

Our treatment of the HGS accounts for changes in the transition frequency $(\Delta\omega)$ and transition dipole $(\Delta\mu)$ relative to the equilibrium ground state, but assumes the dynamics that drive dephasing are unchanged. We note that the vibrational energy deposited into the solvent results in spectral changes to the OH absorption equivalent to a small temperature change after the energy has diffused, and therefore make use of the temperature dependence of the linear OH absorption spectrum to aid in modeling the HGS absorption [Fig. 9(a)]. As the temperature is increased, the line shape shifts to higher frequencies and decreases in intensity without broad-

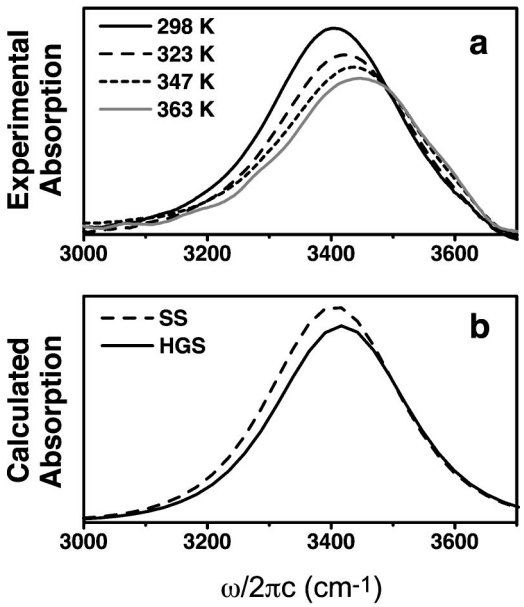

FIG. 9. (a) Experimental temperature-dependent FTIR of 1% HOD in D_2O in the OH stretching region. (b) The steady-state (SS) and hot ground state (HGS) absorption spectra calculated from our model with the extracted dynamical quantities. The HGS spectrum is calculated using $\Delta\omega=12\ \mathrm{cm}^{-1}$, $\Delta\mu=0.05$.

ening significantly. These changes are due to a increase in the fraction of weakened or broken hydrogen bonds. We define the frequency shift of the HGS transition relative to the equilibrium transition as $\Delta\omega=\omega_{10}^{\mathrm{HGS}}-\omega_{10}$ and the change in transition moment between states as $\Delta\mu=(\mu_{10}-\mu_{10}^{\mathrm{HGS}})/\mu_{10}$. The absorption change and frequency shift are found to scale approximately linearly with each other: $|\Delta\mu|^2\approx 0.0075\ \Delta\omega$, where $\Delta\omega$ is measured in cm^{-1}. We use this empirical relationship, valid for temperature dependent spectra of the equilibrium system, to constrain the values of $\Delta\mu$ and $\Delta\omega$ for the inherently nonequilibrium HGS.

The vibrational contribution to the response function, including the harmonic approximations, population relaxation, and the HGS are

$$\begin{aligned}\tilde{R}^{\mathrm{I}}_{\mathrm{vib}}(t_3,t_2,t_1)=|\mu_{10}|^4\left(\frac{i}{\hbar}\right)^3&\exp[-i\omega_{10}(t_3-t_1)]\{\exp[-(t_3+t_1)/2T_1]F^{(3)}_{0101}(t_3,t_2,t_1)\\&+\exp[-(t_3+2t_2+t_1)/2T_1]F^{(4)}_{0101}(t_3,t_2,t_1)-2\exp[-(3t_3+2t_2+t_1)/2T_1]\\&\times\exp[-i(\omega_{21}-\omega_{10})t_3][F^{(2)}_{0121}(t_3,t_2,t_1)]^*-|1-\Delta\mu|^2\exp[-i(\Delta\omega)t_3]\\&\times\exp[-(t_3+t_1)/2T_1][1-\exp(-t_2/T_1)]F^{(3)}_{0101}(t_3,t_2,t_1)\},\end{aligned}\tag{13}$$

$$\begin{aligned}\tilde{R}^{\mathrm{II}}_{\mathrm{vib}}(t_3,t_2,t_1)=|\mu_{10}|^4\left(\frac{i}{\hbar}\right)^3&\exp[-i\omega_{10}(t_3+t_1)]\{\exp[-(t_3+t_1)/2T_1]F^{(1)}_{0101}(t_3,t_2,t_1)\\&+\exp[-(t_3+2t_2+t_1)/2T_1]F^{(2)}_{0101}(t_3,t_2,t_1)-2\exp[-(3t_3+2t_2+t_1)/2T_1]\\&\times\exp[-i(\omega_{21}-\omega_{10})t_3][F^{(4)}_{0121}(t_3,t_2,t_1)]^*-|1-\Delta\mu|^2\exp[-i(\Delta\omega)t_3]\exp[-(t_3+t_1)/2T_1]\\&\times[1-\exp(-t_2/T_1)]F^{(1)}_{0101}(t_3,t_2,t_1)\},\end{aligned}\tag{14}$$

$$\begin{aligned}\tilde{R}^{\mathrm{III}}_{\mathrm{vib/pop}}(t_3,t_2,t_1)=|\mu_{10}|^4\left(\frac{i}{\hbar}\right)^3&\exp[-i\omega_{10}(t_3+t_1)-i\omega_{20}t_2]\\&\times\{2\exp[-(t_3+4t_2+t_1)/2T_1]\\&\times[F^{(1)}_{0121}(t_3,t_2,t_1)]-2\exp[-(3t_3+4t_2\\&+t_1)/2T_1]\exp[-i(\omega_{21}-\omega_{10})t_3]\\&\times[F^{(3)}_{0121}(t_3,t_2,t_1)]^*\}.\end{aligned}\tag{15}$$

Here, we have assumed that the system is initially in the ground state at room temperature, and a harmonic approximation has been used to scale transition matrix elements of the eigenstates ($\mu_{10}=\sqrt{2}\mu_{21}$). Substitution of these expressions, along with the orientational correlation functions into Eq. (7) yields the final expression for the nonlinear polarization.

The nonlinear polarization acts as a source to radiate a signal field $\mathbf{E}_{\mathrm{rad}}\propto\partial\mathbf{P}^{(3)}/\partial t$ into the phase-matched direction $\mathbf{k}_{\mathrm{sig}}$, which is detected in the experiments. The PS experiments employ homodyne detection of an integrated vibrational echo signal

$$\mathbf{S}_E(\mathbf{k}_{\mathrm{sig}},t_\beta,t_\alpha)\propto\int_{-\infty}^{\infty}|\mathbf{E}_{\mathrm{rad}}(\mathbf{k}_{\mathrm{sig}},t_\beta,t_\alpha;t)|^2dt.\tag{16}$$

PP signals are calculated within the framework of a FWM experiment in which two interactions are derived from the pump beam and one from the probe beam. The transmitted probe beam serves as an in-phase local oscillator (LO) because the radiated field propagates in the same direction as the probe. They pass through a bandpass filter before detection, resulting in the heterodyne-detected signal

$$\begin{aligned}&\mathbf{S}_{\mathrm{PP}}(\mathbf{k}_{\mathrm{sig}},\tau)\\&\propto\int_{-\infty}^{\infty}d\omega F(\omega)\mathrm{Re}\left[\int_{-\infty}^{\infty}dt_{\mathrm{LO}}e^{-i\omega t_{\mathrm{LO}}}\right.\\&\left.\times\int_{-\infty}^{\infty}dt\mathbf{E}_{\mathrm{rad}}(\mathbf{k}_{\mathrm{sig}},t_\beta=\tau,t_\alpha=\tau;t)\mathbf{E}_{\mathrm{LO}}(\mathbf{k}_{\mathrm{sig}},t_{\mathrm{LO}};t)\right],\end{aligned}\tag{17}$$

where $F(\omega)$ is the bandpass filter spectrum. For the most part, the present work focuses on the time and polarization dependence of the PP signal for a fixed detection frequency, which primarily measures molecular reorientation and population relaxation.

B. Numerical calculation methods and results

Extraction of the dynamical quantities proceeded by fixing the values of the scalar, static quantities in the expressions above and then iteratively fitting the experimental integrated PS, MA-PP and anisotropy decays to self-consistently determine $C(t)$, T_1 and $p_2(t)$. (Note that the dispersed PS decays in Fig. 3 were not used in this procedure.) The scalar quantities are (1) the frequency of the fundamental transition $\omega_{10}=3400\ \mathrm{cm}^{-1}$, determined from the peak of the linear Fourier transform infrared (FTIR) absorption spectrum of HOD in D_2O; (2) the frequency of the overtone transition $\omega_{21}=3150\ \mathrm{cm}^{-1}$ taken from previous determinations of the anharmonicity;[19] and (3) the frequency

shift $\Delta\omega$ upon thermalization, discussed below. The experimental signals were evaluated with Eqs. (16) and (17), including finite duration pulses expressed in terms of Eq. (6). Calculation of the PS decay included the amplitude and phase of the electric field envelopes that were used to make the measurement, as extracted from the FROG taken immediately afterwards. In both experiments and calculations, we found that pulse characteristics strongly influence the early time decay of the PS signal, which is in agreement with observations made by others.[57] A consistent treatment of the experiment and data is achieved by fitting the calculated integrated echoes with the same Gaussian form as the experimental data. The reorientational correlation function $p_2(t)$ was chosen to be biexponential based on the form of the anisotropy decay, while the initial parameters for the global analysis came from a fit to $r(t)$.

To extract the correlation function from the experimental PS data, we compared the experimental result to the PS signal calculated from a trial correlation function, and then repeatedly adjusted its amplitude and time scales to improve the fit. We constructed a real-valued frequency correlation function from two overdamped and two underdamped Brownian oscillators.[53] These oscillators were initially chosen to correspond to the time scales observed in the experiment and to the librational period of D_2O. The initial trial correlation function was obtained from a fit of the response function to the PS measurement assuming δ function pulses. As an additional constraint to the amplitude of the correlation function, the width of the OH absorption line shape was fit to determine $C(0)$. The line shape is calculated as

$$\sigma(\omega) \propto \mathrm{Re}\left[\int_0^\infty dt \exp[i(\omega-\omega_{10})t - g_{11}(t)] p_1(t) \times \exp(-t/2T_1) \right], \tag{18}$$

where $g_{11}(t)$ is the line shape function defined in the Appendix.

To evaluate quantities relating to the thermalization effects, we examine the behavior of the PP signal for pulse delay times that are long compared with the vibrational dynamics, where it exhibits a positive offset. The magnitude of this offset, $\approx 3.5\%$ of the maximum of the parallel signal, is the same for the parallel, crossed, and magic angle decays detected with the 3400 cm^{-1} filter. It remains constant for delays at least as long as 50 ps. An offset at long times has been observed in previous pump-probe[20,39] and transient grating experiments on water,[29,30] and has been attributed to absorption from the HGS following vibrational relaxation. Stenger and co-workers postulated that the effect could be modeled with a HGS transition that is distinct from the equilibrium fundamental transition only in a frequency shift to the blue ($\Delta\omega = 20\ \mathrm{cm}^{-1}, \Delta\mu = 0$).[29] However, the nonlinear signals calculated with these values do not reproduce our experimental results; the calculated magnitude of the offset in the aforementioned pump probe signal is too small by nearly a factor of 10 (Fig. 5), while the PS signal exhibits an offset that is much too large (~ 6 fs, not shown). The discrepancy results from the dependence of the response functions on the detection frequency. For sufficiently long t_2 delays, the nonlinear signal reflects the difference in the absorption spectra between the equilibrium and HGS fundamental transitions. Because the frequency at which the PP measurement is detected is near the peak of the equilibrium absorption spectrum, this absorption difference is minimal for shifts that are small compared with the linewidth. However, the PS is sensitive to changes in the entire absorption line due to the broadband nature of the detection. The calculated PP signals in Fig. 5 demonstrate that the appropriate frequency shift and associated change in dipole to model the experimental data are $\Delta\omega = 12\ \mathrm{cm}^{-1}$, $\Delta\mu = 0.05$. The calculated equilibrium and HGS spectra for these parameters in our model are plotted in Fig. 9(b).

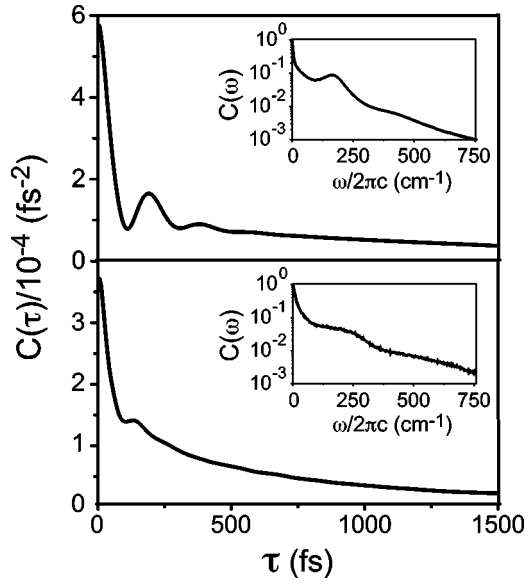

FIG. 10. OH frequency correlation function $C(\tau)$ extracted from fits to the PS and PP measurements (top) compared with that obtained from a model that draws on molecular dynamics computer simulation of HOD in D_2O using the SPC/E model (bottom). (Refs. 31 and 38) The inset in each displays a cosine transform of the respective correlation function.

The final nonlinear signals, calculated from the best fits values of $C(t)$, T_1, and $p_2(t)$ are plotted as solid curves on the experimental data in Figs. 2–6 and 12. The extracted OH frequency correlation function $C(t)$ [Fig. 10(a)] has the same qualitative features as the PS decay, although the relative amplitudes and time scales are different. Its initial decay is faster (50 ± 20 fs), while the oscillation period of the underdamped component (180 ± 20 fs) is slightly longer. The amplitudes of both features are enhanced in the correlation function relative to the PS decay. The slow component of $C(t)$ is 1.4 ± 0.2 ps. The best fit parameters for the extracted frequency correlation function $C(t)$ are given in Table II. The inclusion of more oscillators did not improve comparison to the data. The correlation time for frequency fluctuation, calculated as $\tau_c = C(0)^{-1} \int C(\tau) d\tau$, is $\tau_c = 340$ fs. Not surprisingly, the value of T_1 resulting from our analysis, 700 ± 50 fs, matches the original fit to the MA-PP. Similarly, the resulting form of $p_2(t)$ [Fig. 11(a)] is similar to a direct fit of the anisotropy data except the time scale of the fast component is slightly shorter (50 ± 20 fs and 3.0 ± 0.5 ps).

TABLE II. Best-fit parameters for the Brownian oscillator functions $C_n(t) = A_n \exp(-\gamma_n t)[\cos(\omega_n t)+(\gamma_n/\omega_n)\sin(\omega_n t)]$ that comprise the extracted OH frequency correlation function $C(t)=\Sigma_{n=1}^{4} C_n(t)$.

n	A_n (fs^{-2})	$1/\gamma_n$ (fs)	$\omega_n/2\pi$ (cm^{-1})
1	2.05×10^{-4}	107	···
2	1.03×10^{-4}	1410	···
3	2.47×10^{-4}	104	175
4	2.82×10^{-5}	40	400

The calculations also reproduce most of the trends in the dispersed PS data (Fig. 3), even though the procedure did not explicitly fit these data.

The error bars above reflect the quality of our data and the sensitivity of our fits to each parameter. Because the fastest decay components in both $C(t)$ and $p_2(t)$ occur on the time scale of the pulse duration, the sensitivity of the fits to their precise values is decreased. At long times, the nonlinear signal is reduced by population relaxation and is influenced by the HGS, which affects the homodyne PS decay and the anisotropy. Therefore, we assign the smallest error bars to dynamical quantities associated with times where the pulse overlap is negligible ($\tau_2 > 100$ fs) but the signal remains strong ($\tau_2 < 1.5$ ps).

Finally, we mention an important observation that was not included in the global analysis to extract the dynamical information, but that confirms the results nonetheless. At short delay times, the PP signals contain a weak coherent transient arising from frequency fluctuations, which should roughly follow the form of $C(t)$.[40,58] This transient can be thought of as originating from pump-induced wave packet motion that evolves as a result of intermolecular motions coupled to the OH stretch. It can be most easily observed in the residual that results from subtracting the lifetime and reorientation decays from experimental data averaged over multiple data sets to reduce experimental noise. This residual is plotted with one for the calculated signal, treated in the same way, in Fig. 12. Both residuals exhibit a peak at early times ($\tau_2 \sim 40$ fs) due to the fast decay in the correlation function and a shoulder for $\tau_2 > 100$ fs that is due to the presence of the 180 fs oscillation in the correlation function. Calculations of the pump-probe transient are not able to reproduce this feature using only a biexponential correlation function without the oscillation. We note that $C(t)$ was extracted entirely from the integrated PS results, but still reproduces the early time transient present in the PP data as well as the dispersed PS decays mentioned above.

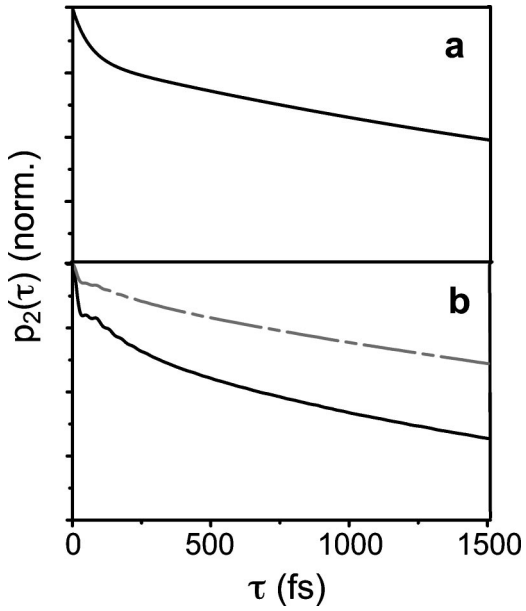

FIG. 11. (a) Normalized OH dipole reorientational correlation function $p_2(\tau)$ extracted from the PP and PS measurements. (b) $p_2(\tau)$ (solid) and $p_1(\tau)$ (dash dot) obtained from molecular dynamics computer simulation of HOD in D_2O using the SPC/E model. (Refs. 32 and 76). Following a ~30 fs librational response and small 140 fs (240 fs) decay, the long time exponential decay of p_2 (p_1) is 1.8 ps (4.1 ps).

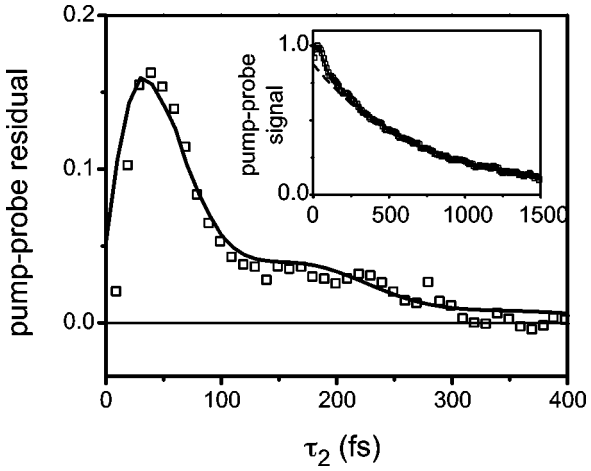

FIG. 12. (Inset) An exponential function whose time scale and amplitude reproduce the long time tail (dash) plotted with the experimental (squares) and simulated parallel pump-probe decays (solid). In the main figure, the residuals that result from subtracting the long time tail from the experimental data (squares) and the model (solid) are plotted.

V. DISCUSSION

A. Vibrational dephasing

In the presence of multiple vibrational dynamics on similar time scales, a unified analysis of multiple nonlinear experiments is required to characterize the frequency fluctuations and spectral diffusion independently of orientational motion and population relaxation. Polarization-selective PP experiments measure population relaxation and reorientation with relatively little influence from dephasing. The PS decay is most sensitive to dephasing because it measures time shifts rather than amplitude changes of the integrated vibrational echoes. Theoretical treatments of dephasing have indicated that the PS decay is linearly proportional to $C(t)$ for τ_2 much greater than τ_c;[59] however, other processes can cause deviations from this relationship when they occur on time scales similar to dephasing. For example, PS calculations of electronic systems found the PS to deviate from $C(t)$ when a finite lifetime was included.[60] In our model, the inclusion of population relaxation and molecular reorientations causes the long time decay of the correlation function to differ from the PS decay. Contributions from the HGS also influence the PS

at long τ_2 delay times. The effect that these processes have on $C(t)$ is made most evident by comparing the results of the present treatment with the correlation function obtained earlier neglecting them.[31] The two are similar, agreeing quantitatively in the time scale and relative amplitudes of all features to within about 20%. The largest two differences are the time scale of the long time component, which has increased from 1.2 to 1.4 ps, and a decrease in $C(0)$.

The experimental correlation function shows three characteristic features, a fast $\sim$60 fs decay, a damped oscillation with a 180 fs period, and a long time monotonic decay of 1.4 ps. The striking feature is the beat, whose time scale indicates that the OH frequency is modulated by underdamped intermolecular motion. This beat corresponds to the pronounced peak at 170 cm^{-1} in the spectral density of $C(t)$ [Fig. 10(a) inset], a feature which coincides with intermolecular resonances present in optical Kerr effect (OKE) or Raman experiments,[4,9,10,61] and in far IR spectra.[62] Comparisons to the spectroscopy of ice and x-ray scattering as well as computer simulation studies, indicate that the 170 cm^{-1} feature is predominantly due to motion of the center of mass of water molecules mostly along the OH coordinate.[63,64] This modulation of the OH frequency implies that the IR spectroscopy of HOD/D_2O reveals underdamped fluctuations in the O–H$\cdots$O hydrogen bond displacement, confirming the long accepted notions that intermolecular fluctuations are underdamped in water, and that a strong correlation exists between the OH vibrational frequency and hydrogen bond distance.[14,65,66] A further comparison of the IR and Raman spectral densities indicates that $C(t)$ is not particularly sensitive to librations, as evidenced by its small amplitude at 400 cm^{-1}. Presumably, motions on the intermolecular potential due to librations do not project well onto the OH coordinate. The fluctuations observed in the locally sensitive OH vibrational spectroscopy can be compared to those intermolecular motions that influence the aqueous solvation of large electronic chromophores in water, which are dominated by contributions from librational motions,[6] although translational oxygen displacement contributes.[12,67]

A number of previous studies have provided characterizations of the OH frequency fluctuations and spectral diffusion for HOD in D_2O. There is limited agreement among these results, partially because various pulse lengths and spectral bandwidth are used, and also a limited set of relaxation effects are considered in modeling. Our results are unique because they characterize the OH vibrational dynamics of HOD in D_2O using pulses fast enough to capture all relevant time scales, and use a model that includes all anticipated vibrational and orientational relaxation processes. Echo experiments, which have employed the shortest pulses, agree that $C(t)$ exhibits a time-scale separation, with $\sim$100 fs fast and $\sim$1 ps slow components.[28–32] For the long time component, values of 700–900 fs have been reported,[28,30] and in one case, an additional 5–15 ps component was also suggested.[29] This falls within the range of values (500–1500 fs) derived from THB.[15,19,23,25] For echo experiments, the short time component is reported to take values from 30–130 fs, although in all but one case this value is extracted using pulses longer than the dynamics. Also, two of the previous echo investigations involved two-pulse techniques,[28] from which extraction of a correlation function is not as reliable as the PS.[68]

The only other study that used pulses shorter than the relevant dynamics investigated the OD dephasing of HOD in H_2O using 2D IR spectroscopy.[33] 2D IR spectra were modeled with a triexponential correlation function with 30 fs, 400 fs, and 1.8 ps components, and no evidence of the 180 fs beat that we observe here. It seems evident that the vibrational dephasing of these isotopically varying species in H_2O and D_2O will differ, but we feel this beat should be largely invariant in the two systems since the molecular dynamics that give rise to it depends more on the electrostatics of the solute-solvent interactions and the mass of the oxygen than the isotopic composition. It is possible that a frequency dependent transition dipole moment in a nonlinear experiment, which is not accounted for in our modeling but is observed to arise from varying hydrogen bonding environments,[65,69] may need to be included for a proper comparison. As an additional point, a study of this short time dynamics requires proper sample handling. We note that the HOD/H_2O data was acquired in a 6 μm path length CaF_2 cell. [When we attempted these experiments in a 50 μm path length CaF_2 cell, the signal only matched results from experiments performed in a jet for waiting times $>$250 rs due to the overwhelming nonresonant response from the cell windows. This response largely masked the novel fast dynamics that we report here.

Computer simulations provide a direct avenue for interpreting our results in terms of molecular quantities. Although water has been the subject of numerous simulation studies, it is unclear how well commonly used classical potentials describe vibrational and intermolecular dynamics and relaxation since they are generally parametrized against thermodynamic and static or time-averaged properties. With the increasing number of experiments sensitive to dynamics, an effort has been made by several groups to use classical MD to simulate the influence of hydrogen bond dynamics on the dephasing and reorientational dynamics measured with time-resolved IR experiments. Simulation of the vibrational dephasing of the normal modes of H_2O embedded in D_2O found a bimodal correlation function with time constants of 50 and 800 fs.[70] Citing the underdamped oxygen velocity autocorrelation function obtained from simulations, Hynes and co-workers indicated that underdamped motion of the hydrogen bond should be observed in IR spectroscopy if the OH stretch frequency ω tracks the hydrogen bond length.[36] The Hynes collaborators,[36,37] Skinner and co-workers,[34,35,71,72] and our own group[31,38] all found a reasonably strong correlation between ω and the hydrogen-bond length R_{OO}, with short strong hydrogen bonds leading to large redshifts in ω and weak or broken hydrogen bonds on the blue side of the line. This result indicates that the experimental correlation between frequency and distance for hydrogen bonding solids holds partially for liquids, and variation of hydrogen bond length should influence the IR spectroscopy. Our simulated frequency correlation function, which is very similar to that of the other groups even with different water potentials, is pictured in Fig. 10(b). It exhibits

the same qualitative features as the experimentally determined $C(t)$: a fast decay, an oscillation at intermediate times, and a long time component. The amplitudes and time scales of the simulated $C(t)$ differ slightly from the experimental values, particularly for the oscillation and slow decay components, but the qualitative agreement suggests that the models adequately capture the molecular origins of dephasing.

Lawrence and Skinner have interpreted these results as indicating that the short time dynamics reflect oscillatory hydrogen bond stretching and the long time decay is due to the dynamics of hydrogen bond breaking and forming.[35] Hynes and co-workers have concluded that the correlation of ω with R_{OO} is relatively poor for the weaker hydrogen bonds, as a result of a broad distribution of hydrogen bond angles.[36,37] This makes the long time decay more difficult to interpret, but nonetheless a result of hydrogen bond breaking and forming dynamics. Similarly, we have used simulations to create atomic probability densities of a range of configurations adopted by the hydrogen bond acceptor molecule, finding that the geometries are relatively restricted on the red side of the OH line shape, but span a large range of distorted hydrogen bonding configurations on the blue side of the line.[38] These results lead us to conclude that the 180 fs beat and short time behavior reflects configurational fluctuations in both distance and angle to the hydrogen bond acceptor.[32] However, since all structural correlations drop off with the same exponential time scale,[31,38] the long time behavior is inherently collective in nature and difficult to assign to specific motions.

Rather than local structural variables, we find that OH frequency shifts are largely electrostatic in nature and can be expressed in terms of the time-varying electric field that arises from surrounding D_2O molecules acting on the OH stretching coordinate Q.[31,38] For this anharmonic OH oscillator, the $\delta\omega$ is proportional to the force projected on Q, which is dominated by the electric field acting on the proton $\vec{E}(t)$:

$$F(t) \approx z_H \hat{r}_{OH} \cdot \vec{E}(t). \tag{19}$$

Here z_H is the charge on the proton. If we define an OH dipole as $\vec{\mu}_{OH} = -z_H \hat{r}_{OH} Q$, the system-bath interaction in our picture is written as a Stark-shift Hamiltonian

$$H_{SB}(t) \approx F(t) Q = -\vec{\mu}_{OH} \cdot \vec{E}(t). \tag{20}$$

Since the field on the proton dominates the frequency shift, we find a strong correlation between ω and the local electric field due to the hydrogen-bonding partner E_0. This explains the sensitivity of ω to the hydrogen-bond length and the lesser influence of the angle. The remaining molecules in the first solvation shell that do not directly bond to the proton have little influence on the correlation of electric field with ω. Inclusion of the field of all molecules in the simulation (and their periodic images) E yields an almost perfect correlation to ω, leading us to conclude that there are both local and collective origins to the frequency fluctuations. The correlation functions for these order parameters help describe the molecular origins of vibrational dephasing. While $C(t)$ is best reproduced by the total electric field autocorrelation function $C_E(t) = \langle E(t)E(0) \rangle$ for all times investigated, at short times the local electric field autocorrelation function $C_{E_0}(t) = \langle E_0(t)E_0(0) \rangle$ also resembles $C(t)$ and reproduces the oscillation particularly well. We conclude that this feature is largely a signature of local configurational changes, because it is also observed in the dynamics of R_{OO}, indicating that hydrogen bond stretching is an important component of frequency fluctuations at short times.

Our modeling from MD simulations finds that all time correlation functions investigated for structural and collective order parameters decay asymptotically on the same long time scale.[31,38] As a consequence, the long-time decay of frequency correlations cannot be associated with the dynamics of a specific motion of individual molecules, but rather it arises from various contributions reflecting collective rearrangements of molecules in the hydrogen bond network, hydrogen bond breaking and forming, as well as fluctuations in density and polarization fields[73] on length scales greater than a molecular diameter. Previous time-resolved infrared studies on hydride stretching vibrations in protic liquids have suggested that the long time relaxation behavior observes hydrogen bond breaking and/or forming dynamics.[23,25] We differ in this conclusion if ''dynamics'' is meant to refer to a structurally resolved characterization of how a hydrogen bond breaks or forms. Molecular dynamics simulations have established that hydrogen bond making or breaking coordinates involve many-body reorganization, and cannot be simply expressed in terms of local variables such as the hydrogen bond distance and angle. It is therefore to be expected that intermolecular variables that dictate ω do not project well onto the coordinate for hydrogen bond breaking. Drawing on the findings of our modeling,[31,38] we conclude that ultrafast infrared spectroscopy on time scales longer than the correlation time for frequency fluctuations is not a structurally sensitive probe, but rather characterizes the kinetics of randomizing intermolecular hydrogen bonding structure. Sensitivity to molecular dynamics is lost on dephasing and only an effective rate constant is measured.

The finding that the molecular electric field is the definitive variable that describes OH vibrational dephasing has implications when comparing studies in H_2O and D_2O. For the Stark-effect Hamiltonian given in Eq. (20), the frequency shift is obtained from matrix elements of Q in the system eigenstates: $\delta\omega = -z_H E(\langle 1|Q|1\rangle - \langle 0|Q|0\rangle)/\hbar$. Evaluating $\delta\omega$ will depend on the reduced mass of Q, which differs considerably for studies of the OH stretch of HOD/D_2O and for the OD stretch of HOD/H_2O. We find that evaluating the matrix elements in Q for a Morse well leads to a $\sim\sqrt{2}$ scaling for $\delta\omega_{OH}/\delta\omega_{OD}$. This explains the large variation in OH and OD linewidths for HOD/D_2O ($260\ cm^{-1}$) and HOD/H_2O ($160\ cm^{-1}$).

B. Molecular reorientation

With respect to reorientational data, the long time component of our anisotropy matches the reorientational dynamics measured by other groups.[17,21] There have been reports of a >10 ps contribution to the anisotropy,[17,74] which is well beyond the noise sensitivity of our measurement. There are

also suggestions of coupling between rotational motion and H bonds leading to spectrally varying reorientation.[21,75] We find no need to include such effects in modeling the dynamics we observe. This is not surprising given the fast OH frequency correlation time and the broadband nature of our experiment.

The fast 50 fs decay in $p_2(\tau)$ has not been resolved in previous IR experiments, and is consistent with librations, hindered rotational motion of individual OH dipoles. This differs from Raman measurements that probe the many-body polarizability. Even though the observation is made through the reorientation of individual OH dipoles, the dynamics giving rise to this librational motion is inherently collective.[2,3,64]

In Fig. 11 we compare the $p_\ell(t)$ reorientational dynamics of the OH vector measured by our experiments to those obtained from classical MD simulations of HOD in D_2O using the SPC/E model.[32,76] These results from simulation are similar to others on HOD in D_2O,[35] as well as earlier work on neat D_2O.[1,77] The rotational time correlation function $p_2(t)$, which exhibits little dependence on the particular model used for the calculation, decays rapidly with 30 and 140 fs time constants and a weak oscillation near 80 fs, prior to a long time exponential decay. The short time decay and oscillation has been universally assigned to librations, which is clearly nondiffusive due to a restoring force imposed by the relatively static configuration of surrounding solvent molecules on the libration time scale. Our experiments clearly reveal a fast librational contribution to $p_2(t)$, however, our 45 fs pulses are still not short enough to determine whether this behavior is weakly underdamped as the simulations predict.

For the asymptotic long time decay of $p_\ell(t)$ from simulations, we find decays on 4.1 ps ($\ell=1$) and 1.8 ps ($\ell=2$) time scales, which suggests adequate agreement to the scaling factor of $\ell(\ell+1)$ predicted for reorientational diffusion. However, the initial decay time and oscillation period are relatively independent of the order of the Legendre polynomial. Deviation from diffusion scaling is not surprising at short times when atomic interactions are still important. Although the results of our modeling assumed a scale factor of three between $\ell=1$ and $\ell=2$, performing the calculations without scaling the short time component produced a very similar result.

Other experimental techniques are sensitive to molecular reorientations and the intermolecular dynamics that influence the correlation function. Collective librational motions have been observed in low-frequency Raman[61] and OKE experiments,[9,10] and attributed to the dominant fast decay in aqueous solvation dynamics experiments.[6,12] OKE, NMR, and dielectric relaxation all observe diffusive reorientational relaxation. OKE experiments have measured a 1.2 ps component in the correlation function of D_2O,[11] and values of 2–3 ps from NMR matches our measurement.[78] Dielectric relaxation[79] and time-domain terahertz spectroscopy[80] find a relaxation time of 8 ps, although these resonant experiments are sensitive to $p_1(t)$. Discrepancies in these results are primarily due to the collective nature of many of the other experiments, as opposed to IR spectroscopy that directly probes the OH dipole on individual molecules. For example, Raman and OKE spectroscopy measures a correlation function of the many-body polarizability, which includes terms from single molecules as well as interaction-induced terms that depend on an arbitrarily large number of molecules.[10]

C. Vibrational population relaxation

The 700 fs population lifetime that we extract from our measurements agrees well with the values of 740 and 700 fs measured by the Bakker[18–20] and Wiersma[81] groups. Gale and co-workers initially reported a frequency dependent lifetime varying from 500 fs to 1 ps,[24] although subsequent analysis that also treated spectral and orientational relaxation in the data is consistent with a constant value of 1.3 ps.[23,25,26] These numbers are shorter than those measured with longer IR pulse durations on the order of T_1.[15,17,27] Considering our 340 fs frequency correlation time, we conclude that if spectrally varying population relaxation does exist, it must represent a fractionally small contribution to the ensemble.

The origin and pathways for vibrational relaxation for HOD/D_2O and other isotopic variants has recently been reviewed.[82] Several experimental and theoretical investigations have identified the predominant energy relaxation pathways from $\nu=1$ of the OH stretch of HOD/D_2O, concluding that this occurs mainly through intramolecular relaxation pathways, primarily through the HOD bend overtone.[27,71,83] Additionally, Bakker has argued that the O–H$\cdots$O coordinate is the primary intermolecular accepting mode for vibrational relaxation.[20] From a classical perspective, the OH vibrational relaxation is driven by those fluctuating forces acting on the OH coordinate that couple it to accepting coordinates of the molecule and surroundings. For this system, these forces arise from the same electrostatic interactions that drive vibrational dephasing,[84] although for the case of vibrational relaxation, these are fluctuating forces at the energy gap which separates two different anharmonic states.[82] This conclusion reinforces the consistent observation that Coulombic interactions are largely responsible for vibrational relaxation processes for diatomic and polyatomic solutes in water.[85]

As in our present work, earlier experimental and theoretical work on OH vibrational relaxation in water has always accounted for vibrational relaxation through an exponential rate determined from golden rule expressions that assume a fast bath. Although this does seem to work well in the modeling of our data, it is not clear that a Markovian approximation is valid in this system. The frequency correlation time is only a factor of 2 smaller than the lifetime, and the long time decay of $C(t)$ exceeds T_1 by a factor of 2. These observations suggest that future investigations into the vibrational energy relaxation in this system should consider models beyond the weak interactions between the system and a fast bath, and a separation of coherence and population relaxation. Studies of this sort are just now being reported.[86]

D. Thermalization effects

Several time-resolved infrared studies of hydride stretching vibrations in hydrogen-bonding liquids have now firmly established that observables on picosecond time scales are

influenced by changes in the optical properties of the OH or OD transition that arise on vibrational relaxation.[29,30,39,81,87,88] Terms such as ''hot ground state,'' ''thermalization effect,'' and ''photoproduct'' are used to describe a relaxation-induced spectral shift or increase of intensity in a region of the spectrum associated with weaker or broken hydrogen bonds, which is consistent with the spectral changes observed on raising the temperature of the sample. The physical basis for this change is almost certainly a nonnegligible transfer of kinetic energy from the system (OH oscillator) to the bath, which in turn affects the fluctuating environment about the HOD molecule. This process, however, is inherently nonequilibrium due to the short time scale for relaxation. Therefore, the vibrational dynamics on time scales relevant to the HGS ($>1-2$ ps) should not be interpreted in terms of equilibrium hydrogen bond dynamics unless a linear response argument is invoked (the validity of which may be questionable).[89]

The most detailed previous work on the thermalization process comes from PS studies using pulses of 70–150 fs. Stenger and co-workers found a large recurrence at 2 ps in the PS for pulses centered on the red side of the OH absorption line, but not on the blue.[29] This is possible to observe with pulses that have a narrow spectral bandwidth compared to the absorption profile. Similarly, Pshenichnikov and co-workers, see a recurrence at 2 ps using pulses centered to the red ($\sim 3300\ \mathrm{cm}^{-1}$).[30,81] We do not observe this long time recurrence in our data. This is due to the broadband excitation and probing in our experiments, which integrates over all frequencies, lessening the overall effect on the PS decay below our signal to noise level at long waiting times. Stenger *et al.* attributed the rise in signal to an absorption process from a hot ground state that grows in with the vibrational lifetime, and were able to reproduce it on the blue side of the band with proper choice of $\Delta\omega$, assuming $\Delta\mu=0$. However, the signal calculated on the red side of the line also exhibited a recurrence that was stronger than they observed experimentally. We suspect that their results could be reproduced globally by adopting the values of $\Delta\omega$ and $\Delta\mu$ used in our modeling. Pshenichnikov has emphasized that relaxation observed in homodyne detected experiments such as PS and transient gratings primarily reflects changes in the refractive index of the sample, rather than changes in absorption.[30,81] The results of Pshenichnikov and the recent pump-probe experiments on HOD/H_2O by Steinel and co-workers are consistent with a long time picosecond spectral change in the absorption spectrum equivalent to raising the temperature of the sample by $1-2\ ^\circ\mathrm{C}$.[30,88] Our obtained values for $\Delta\omega$ and $\Delta\mu$ are consistent with changes in the steady state FTIR spectrum in which the temperature has been raised roughly 10°. This relatively large change in temperature compared to what would be expected from the energy deposited by the pump pulse is likely due to the nonequilibrium distribution of bath states that are excited upon vibrational relaxation.

As for the specific model we have chosen for the thermalization process, we do not claim at this point that it is rigorously correct, but it reproduces our data well and may well reproduce data others have published. Even though our PS data does not show a picosecond recurrence such as those of Stenger and Pshenichnikov, our results should not be considered inconsistent, since our modeling draws a similar response function. Also, the long time behavior of the PS under influence of the HGS strongly depends on the pulse length and spectral bandwidth used, which in our case is considerably shorter in length and spectrally broader. Calculations of PS measurements show that longer pulses with narrower bandwidth give more pronounced recurrences in PS measurements, and the effect should be imperceptible for 30 fs pulses.[90]

VI. SUMMARY AND CONCLUSIONS

We have presented a comprehensive investigation of the vibrational dynamics of the OH stretch of HOD in D_2O, in which PS experiments, polarization-selective PP experiments, and a unified response function analysis allowed the separation of pure dephasing (frequency fluctuations and spectral diffusion), reorientational motions, vibrational population relaxation, and thermalization effects. Use of ultrashort IR pulses whose transform-limited bandwidth spans the entire OH absorption ensures that all of the dynamical processes in this system are captured. On picosecond time scales our measurements are consistent with the findings of others, but we reveal new signatures of the dynamics of hydrogen bonds on the fastest femtosecond time scales.

The vibrational dephasing and molecular reorientational dynamics measured in our experiments both exhibit a clear separation of fast and slow time scales, which are conveniently divided by the correlation time $\tau_c \sim 340$ fs. We view this time scale separation also as a separation of the observables in infrared experiments into dynamic and kinetic regimes. In both cases, MD simulations indicated that the intermolecular dynamics that contribute to the observable for times shorter than τ_c are characteristic of local processes—low amplitude motions that occur on molecular length scales. These include ~ 180 fs underdamped fluctuations through various hydrogen bonding configurations, and shorter time scale librational motion. On time scales longer than the correlation time, dephasing and reorientations are diffusive. These are large-scale motions, exchange of local partners, and diffusion that result from collective reorganizations of the hydrogen bond network. These dynamics fit well within the energy landscape picture for water, where the system samples local minima of the global potential energy (inherent structures) on short time scales, but undergoes transitions between basins of attraction in the surface on longer time scales corresponding to collective structural changes.[3,91] When viewed through the IR spectroscopy, the long time behavior loses its sensitivity to the molecular hydrogen-bonding dynamics. The inherently collective motions associated with the reorganization of the liquid involve a coordinate that does not project favorably onto the OH stretching frequency. Therefore the long time behavior may be related to hydrogen bond making and breaking, but only in a nonspecific sense as a kinetic rate for randomizing structures.

Even though the experiments, in our view, are not directly sensitive to dynamics over all time periods, the comparison between the experiment and predictions from classical molecular dynamics simulations is very favorable. This

indicates the vital role that molecular dynamics simulations play in interpreting the underlying dynamic information in IR experiments. Conversely, ultrafast IR experiments such as these provide a set of experimentally determined standards that can be used as a point of comparison to particular models of water by how they predict vibrational dephasing, population relaxation and molecular reorientation. Presently, there is already excellent agreement from a qualitative perspective, suggesting that simple rigid water potentials do well in reproducing dynamic features. A quantitative comparison with different water models will offer insight into which molecular interactions in water are of particular importance for hydrogen-bonding dynamics.

In extracting this information, we have used a fairly conventional model for the molecular response function, which reproduces and predicts the features in several different experiments based on just a limited set of variables that describe the behavior of HOD in D_2O. However, we note that the experiments presented here used broadband pulses to excite the entire distribution of OH frequencies, and therefore the dynamics that they measure are averaged over all solvent configurations. Others have noted that the intermolecular dynamics in water may depend on local environment due to the strong influence of hydrogen bonds, leading to a distribution of time scales for local and structural reorganizations. The experiments performed here are fairly insensitive to this behavior and our theoretical modeling has correspondingly assumed that the frequency fluctuations follow Gaussian statistics. Based on the short frequency correlation time obtained and no clear indication of nonexponential relaxation behavior in our data, we suspect that spectrally varying dynamics for HOD/D_2O are a fairly small and short lived effect. Studies of heterogeneous hydrogen-bonding dynamics are nonetheless very important, and the ensemble-averaged treatment in this paper forms a point of departure for future investigations of spectrally varying dynamics using two-dimensional infrared spectroscopy.[92]

ACKNOWLEDGMENTS

The authors have greatly benefited from numerous discussions on the molecular dynamics of water and the microscopic origin of OH vibrational dephasing with Joel Eaves and Phillip Geissler. They also thank Joel Eaves for providing the simulation results in this paper. They thank David Jonas for providing source code for simulating nonlinear signals that guided the initial development of our own code, and Maxim Pshenichnikov and Sergey Yeremenko for discussions on thermalization. This work was supported by Basic Energy Sciences of the U.S. Department of Energy Grant No. (DE-FG02-99ER14988), the Laser Research Facility at MIT Grant No. (NSF CHE-0111370), and the David and Lucile Packard Foundation. J.J.L. thanks the DOD for an NDSEG fellowship.

APPENDIX

The frequency fluctuations for the three-level anharmonic oscillator are described within the framework given by Ref. 50. We begin by defining the line shape function

$$g_{pq}(t)=\int_0^t d\tau_2 \int_0^{\tau_2} d\tau_1 C_{pq}(\tau_2-\tau_1), \tag{A1}$$

where the frequency correlation function C_{pq} was given in Eq. (9). Then, the dephasing functions can be written as

$$\begin{aligned}-\ln F^{(1)}_{0101}(t_3,t_2,t_1)=&\, g_{11}(t_1)+g_{11}(t_2)+g_{11}(t_3)\\ &-g_{11}(t_1+t_2)-g_{11}(t_2+t_3)\\ &+g_{11}(t_1+t_2+t_3),\end{aligned} \tag{A2}$$

$$\begin{aligned}-\ln F^{(2)}_{0101}(t_3,t_2,t_1)=&\, g_{11}(t_1)+g^*_{11}(t_2)+g^*_{11}(t_3)\\ &-g_{11}(t_1+t_2)-g^*_{11}(t_2+t_3)\\ &+g_{11}(t_1+t_2+t_3),\end{aligned} \tag{A3}$$

$$\begin{aligned}-\ln[F^{(3)}_{0101}(t_3,t_2,t_1)]^*=&\, g_{11}(t_1)-g_{11}(t_2)+g^*_{11}(t_3)\\ &+g_{11}(t_1+t_2)+g_{11}(t_2+t_3)\\ &-g_{11}(t_1+t_2+t_3),\end{aligned} \tag{A4}$$

$$\begin{aligned}-\ln[F^{(4)}_{0101}(t_3,t_2,t_1)]^*=&\, g_{11}(t_1)-g^*_{11}(t_2)+g_{11}(t_3)\\ &+g_{11}(t_1+t_2)+g^*_{11}(t_2+t_3)\\ &-g_{11}(t_1+t_2+t_3),\end{aligned} \tag{A5}$$

$$\begin{aligned}-\ln F^{(1)}_{0121}(t_3,t_2,t_1)=&\, g_{11}(t_1)-g_{21}(t_1)+g_{11}(t_2)\\ &-g_{12}(t_2)-g_{21}(t_2)+g_{22}(t_2)\\ &+g_{11}(t_3)-g_{12}(t_3)-g_{11}(t_1+t_2)\\ &+g_{21}(t_1+t_2)-g_{11}(t_2+t_3)\\ &+g_{12}(t_2+t_3)+g_{11}(t_1+t_2+t_3),\end{aligned} \tag{A6}$$

$$\begin{aligned}-\ln F^{(2)}_{0121}(t_3,t_2,t_1)=&\, g_{11}(t_1)+g^*_{11}(t_2)-g^*_{12}(t_2)\\ &+g^*_{11}(t_3)-g^*_{12}(t_3)-g^*_{21}(t_3)\\ &+g^*_{22}(t_3)-g_{11}(t_1+t_2)\\ &+g_{21}(t_1+t_2)-g^*_{11}(t_2+t_3)\\ &+g^*_{12}(t_2+t_3)+g_{11}(t_1+t_2+t_3)\\ &-g_{21}(t_1+t_2+t_3),\end{aligned} \tag{A7}$$

$$\begin{aligned}-\ln[F^{(3)}_{0121}(t_3,t_2,t_1)]^*=&\, g_{11}(t_1)-g_{21}(t_1)-g_{11}(t_2)\\ &+g_{12}(t_2)+g^*_{11}(t_3)-g^*_{12}(t_3)\\ &+g_{11}(t_1+t_2)+g_{11}(t_2+t_3)\\ &-g_{12}(t_2+t_3)-g_{21}(t_2+t_3)\\ &+g_{22}(t_2+t_3)-g_{11}(t_1+t_2+t_3)\\ &+g_{21}(t_1+t_2+t_3),\end{aligned} \tag{A8}$$

$$
\begin{aligned}
-\ln[F^{(4)}_{0121}(t_3,t_2,t_1)]^* = {} & g_{11}(t_1) - g^*_{11}(t_2) + g^*_{12}(t_2) \\
& + g_{11}(t_3) - g_{12}(t_3) - g_{21}(t_3) \\
& + g_{22}(t_3) + g_{11}(t_1+t_2) \\
& - g_{21}(t_1+t_2) + g^*_{11}(t_2+t_3) \\
& - g^*_{12}(t_2+t_3) - g_{11}(t_1+t_2+t_3) \\
& + g_{21}(t_1+t_2+t_3). \qquad \text{(A9)}
\end{aligned}
$$

[1] A. Rahman and F. H. Stillinger, J. Chem. Phys. **55**, 3336 (1971).
[2] I. Ohmine and H. Tanaka, Chem. Rev. (Washington, D.C.) **93**, 2545 (1993).
[3] I. Ohmine and S. Saito, Acc. Chem. Res. **32**, 741 (1999).
[4] G. E. Walrafen, J. Chem. Phys. **40**, 3249 (1964).
[5] W. Jarzeba, G. C. Walker, A. E. Johnson, M. A. Kahlow, and P. F. Barbara, J. Phys. Chem. **92**, 7039 (1988).
[6] R. Jimenez, G. R. Fleming, P. V. Kumar, and M. Maroncelli, Nature (London) **369**, 471 (1994).
[7] P. Bosi, F. Dupre, F. Menzinger, F. Sacchetti, and M. C. Spinelli, Lett. Nuovo Cimento Soc. Ital. Fis. **21**, 436 (1978); J. Teixeira, M.-C. Bellissent-Funel, and S. H. Chen, J. Phys.: Condens. Matter **2**, 105 (1990).
[8] D. W. G. Smith and J. G. Powles, Mol. Phys. **10**, 451 (1966).
[9] E. W. Castner, Jr., Y. J. Chang, Y. C. Chu, and G. E. Walrafen, J. Chem. Phys. **102**, 653 (1995); S. Palese, L. Schilling, R. J. D. Miller, P. R. Staver, and W. T. Lotshaw, J. Phys. Chem. **98**, 6308 (1994).
[10] C. J. Fecko, J. D. Eaves, and A. Tokmakoff, J. Chem. Phys. **117**, 1139 (2002).
[11] K. Winkler, J. Lindner, H. Bürsing, and P. Vühringer, J. Chem. Phys. **113**, 4674 (2000).
[12] M. J. Lang, X. J. Jordanides, X. Song, and G. R. Fleming, J. Chem. Phys. **110**, 5884 (1999).
[13] E. T. J. Nibbering and T. Elsaesser, Chem. Rev. (Washington, D.C.) **104**, 1887 (2004).
[14] A. Novak, in *Structure and Bonding*, edited by J. D. Dunitz, P. Hemmerich, R. H. Holm, J. A. Ibers, C. K. Jorgenson, J. B. Neilands, D. Reinen, and R. J. P. Williams (Springer, New York, 1974), Vol. 18, p. 177; W. Mikenda, J. Mol. Struct. **147**, 1 (1986).
[15] R. Laenen, C. Rauscher, and A. Laubereau, J. Phys. Chem. B **102**, 9304 (1998).
[16] R. Laenen, K. Simeonidis, and A. Laubereau, J. Phys. Chem. B **106**, 408 (2002).
[17] R. Laenen, K. Simeonidis, and A. Laubereau, Bull. Chem. Soc. Jpn. **75**, 925 (2002).
[18] S. Woutersen, U. Emmerichs, H.-K. Nienhuys, and H. J. Bakker, Phys. Rev. Lett. **81**, 1106 (1998).
[19] S. Woutersen and H. J. Bakker, Phys. Rev. Lett. **83**, 2077 (1999).
[20] H. K. Nienhuys, S. Woutersen, R. A. v. Santen, and H. J. Bakker, J. Chem. Phys. **111**, 1494 (1999).
[21] H.-K. Nienhuys, R. A. van Santen, and H. J. Bakker, J. Chem. Phys. **112**, 8487 (2000); G. Gallot, S. Bratos, S. Pommeret, N. Lascoux, J.-C. Leicknam, M. Kozinski, W. Amir, and G. M. Gale, *ibid.* **117**, 11301 (2002).
[22] H. J. Bakker, H.-K. Nienhuys, G. Gallot, N. Lascoux, G. M. Gale, J.-C. Leicknam, and S. Bratos, J. Chem. Phys. **116**, 2592 (2002).
[23] G. M. Gale, G. Gallot, F. Hache, N. Lascoux, S. Bratos, and J.-C. Leicknam, Phys. Rev. Lett. **82**, 1068 (1999).
[24] G. M. Gale, G. Gallot, and N. Lascoux, Chem. Phys. Lett. **311**, 123 (1999).
[25] S. Bratos, G. M. Gale, G. Gallot, F. Hache, N. Lascoux, and J.-C. Leicknam, Phys. Rev. E **61**, 5211 (2000).
[26] G. Gallot, N. Lascoux, G. M. Gale, J.-C. Leicknam, S. Bratos, and S. Pommeret, Chem. Phys. Lett. **341**, 535 (2001).
[27] J. C. Deak, S. T. Rhea, L. K. Iwaki, and D. D. Dlott, J. Phys. Chem. A **104**, 4866 (2000).
[28] J. Stenger, D. Madsen, P. Hamm, E. T. J. Nibbering, and T. Elsaesser, Phys. Rev. Lett. **87**, 027401 (2001); S. Yeremenko, M. S. Pshenichnikov, and D. A. Wiersma, Chem. Phys. Lett. **369**, 107 (2003).
[29] J. Stenger, D. Madsen, P. Hamm, E. T. J. Nibbering, and T. Elsaesser, J. Phys. Chem. A **106**, 2341 (2002).
[30] M. S. Pshenichnikov, S. Yeremenko, and D. A. Wiersma, in *Femtochemistry and Femtobiology: Ultrafast Events in Molecular Science*, edited by M. M. Martin and J. T. Hynes (Elsevier, Amsterdam, 2004).
[31] C. J. Fecko, J. D. Eaves, J. J. Loparo, A. Tokmakoff, and P. L. Geissler, Science **301**, 1698 (2003).
[32] J. J. Loparo, C. J. Fecko, J. D. Eaves, S. T. Roberts, and A. Tokmakoff, Phys. Rev. B **70**, 180201.
[33] J. B. Asbury, T. Steinel, C. Stromberg, S. A. Corcelli, C. P. Lawrence, J. L. Skinner, and M. D. Fayer, J. Phys. Chem. A **108**, 1107 (2004).
[34] C. P. Lawrence and J. L. Skinner, Chem. Phys. Lett. **369**, 472 (2003).
[35] C. P. Lawrence and J. L. Skinner, J. Chem. Phys. **118**, 264 (2003).
[36] R. Rey, K. B. Moller, and J. T. Hynes, J. Phys. Chem. A **106**, 11993 (2002).
[37] K. B. Moller, R. Rey, and J. T. Hynes, J. Phys. Chem. A **108**, 1275 (2004).
[38] J. D. Eaves, A. Tokmakoff, and P. Geissler, J. Phys. Chem. B (unpublished).
[39] A. J. Lock, S. Woutersen, and H. J. Bakker, J. Phys. Chem. A **105**, 1238 (2001).
[40] T. Joo, Y. Jia, J.-Y. Yu, M. J. Lang, and G. R. Fleming, J. Chem. Phys. **104**, 6089 (1996).
[41] W. P. de Boeij, M. S. Pshenichnikov, and D. A. Wiersma, Annu. Rev. Phys. Chem. **49**, 99 (1998).
[42] P. Hamm, M. Lim, and R. M. Hochstrasser, Phys. Rev. Lett. **81**, 5326 (1998).
[43] K. Ohta, H. Maekawa, and K. Tominaga, J. Phys. Chem. A **108**, 1333 (2004).
[44] C. J. Fecko, J. J. Loparo, and A. Tokmakoff, Opt. Commun. **241**, 521 (2004).
[45] R. Trebino, K. W. DeLong, D. N. Fittinghoff, J. N. Sweetser, M. A. Krumbugel, B. A. Richman, and D. J. Kane, Rev. Sci. Instrum. **68**, 3277 (1997).
[46] N. Demirdöven, M. Khalil, O. Golonzka, and A. Tokmakoff, Opt. Lett. **27**, 433 (2002).
[47] M. Khalil, N. Demirdüven, and A. Tokmakoff, J. Phys. Chem. A **107**, 5258 (2003).
[48] D. S. Larsen, K. Ohta, Q.-H. Xu, M. Cyrier, and G. R. Fleming, J. Chem. Phys. **114**, 8008 (2001).
[49] A. Tokmakoff, J. Chem. Phys. **105**, 1 (1996).
[50] J. Sung and R. J. Silbey, J. Chem. Phys. **115**, 9266 (2001).
[51] J. Sung and R. J. Silbey, J. Chem. Phys. **118**, 2443 (2003).
[52] S. Mukamel and R. F. Loring, J. Opt. Soc. Am. B **3**, 595 (1986).
[53] S. Mukamel, *Principles of Nonlinear Optical Spectroscopy* (Oxford University Press, New York, 1995).
[54] A. W. Albrecht, J. D. Hybl, S. M. Gallagher Faeder, and D. M. Jonas, J. Chem. Phys. **111**, 10934 (1999).
[55] D. W. Oxtoby and S. A. Rice, Chem. Phys. Lett. **42**, 1 (1976); D. J. Diestler, *ibid.* **39**, 39 (1976).
[56] J. T. Fourkas, H. Kawashima, and K. A. Nelson, J. Chem. Phys. **103**, 4393 (1995); M. Khalil and A. Tokmakoff, Chem. Phys. **266**, 213 (2001).
[57] K. Ohta, D. S. Larsen, M. Yang, and G. R. Fleming, J. Chem. Phys. **114**, 8020 (2001).
[58] D. A. Farrow, A. Yu, and D. M. Jonas, J. Chem. Phys. **118**, 9348 (2003).
[59] G. R. Fleming and M. Cho, Annu. Rev. Phys. Chem. **47**, 109 (1996).
[60] M. Yang, K. Ohta, and G. R. Fleming, J. Chem. Phys. **110**, 10243 (1999).
[61] G. E. Walrafen, in *Water: A Comprehensive Treastise*, edited by F. Franks (Plenum, New York, 1972), Vol. 1, p. 151.
[62] J. B. Hasted, S. K. Husain, F. A. M. Frescura, and J. R. Birch, Chem. Phys. Lett. **118**, 622 (1985).
[63] G. E. Walrafen, M. R. Fischer, M. S. Hokmabadi, and W.-H. Yang, J. Chem. Phys. **85**, 6970 (1986); P. L. Silvestrelli, M. Bernasconi, and M. Parrinello, Chem. Phys. Lett. **277**, 478 (1997).
[64] M. Cho, G. R. Fleming, S. Saito, I. Ohmine, and R. M. Stratt, J. Chem. Phys. **100**, 6672 (1994).
[65] G. C. Pimentel and A. L. McClellan, *The Hydrogen Bond* (Freeman, San Francisco, 1960).
[66] G. L. Hofacker, Y. Marechal, and M. A. Ratner, in *The Hydrogen Bond. I. Theory*, edited by P. Schuster, G. Zundel, and C. Sandorfy (North-Holland, New York, 1976), Vol. 1, p. 296.
[67] N. Nandi, S. Roy, and B. Bagchi, J. Chem. Phys. **102**, 1390 (1995).
[68] A. Piryatinski, C. P. Lawrence, and J. L. Skinner, J. Chem. Phys. **118**, 9664 (2003).
[69] M. G. Sceats and K. Belsley, Mol. Phys. **40**, 1389 (1980).
[70] M. Diraison, Y. Guissani, J.-C. Leicknam, and S. Bratos, Chem. Phys. Lett. **258**, 348 (1996).
[71] C. P. Lawrence and J. L. Skinner, J. Chem. Phys. **117**, 5827 (2002).
[72] S. A. Corcelli, C. P. Lawrence, and J. L. Skinner, J. Chem. Phys. **120**, 8107 (2004).

[73] Y. Georgievskii and R. A. Marcus, J. Phys. Chem. A **105**, 2281 (2001).
[74] S. Woutersen, U. Emmerichs, and H. J. Bakker, Science **278**, 658 (1997).
[75] H. J. Bakker, S. Woutersen, and H.-K. Nienhuys, Chem. Phys. **258**, 233 (2000).
[76] J. D. Eaves, Ph.D thesis, Massachusetts Institute of Technology, 2004.
[77] R. W. Impey, P. A. Madden, and I. R. McDonald, Mol. Phys. **46**, 513 (1982).
[78] B. M. Fung and T. W. McGaughy, J. Chem. Phys. **65**, 2970 (1976); J. Ropp, C. P. Lawrence, T. C. Farrar, and J. Skinner, J. Am. Chem. Soc. **123**, 8047 (2001).
[79] J. Barthel, K. Bachhuber, R. Buchner, and H. Hetzenauer, Chem. Phys. Lett. **165**, 369 (1990); R. Buchner, J. Barthel, and J. Stauber, *ibid.* **306**, 57 (1999).
[80] C. Rønne, P.-O. Åstrand, and S. R. Keiding, Phys. Rev. Lett. **82**, 2888 (1999).
[81] M. S. Pshenichnikov, S. Yeremenko, and D. A. Wiersma, in *Ultrafast Phenomena XIV*, edited by T. Kobayashi, T. Okada, T. Kobayashi, K. A. Nelson, and S. DeSilvestri (Springer, Berlin, 2005).
[82] R. Rey, K. B. Moller, and J. T. Hynes, Chem. Rev. (Washington, D.C.) **104**, 1915 (2004).
[83] R. Rey and J. T. Hynes, J. Chem. Phys. **104**, 2356 (1996); C. P. Lawrence and J. L. Skinner, *ibid.* **119**, 1623 (2003).
[84] J. T. Hynes and R. Rey, in *Ultrafast Infrared and Raman Spectroscopy*, edited by M. D. Fayer (Marcel Dekker, New York, 2001).
[85] R. M. Whitnell, K. R. Wilson, and J. T. Hynes, J. Chem. Phys. **96**, 5354 (1992); R. Rey and J. T. Hynes, *ibid.* **108**, 142 (1998).
[86] S. Yang, J. Shao, and J. Cao, J. Chem. Phys. **121**, 11250 (2004).
[87] J. B. Asbury, T. Steinel, C. Stromberg, K. J. Gaffney, I. R. Piletic, A. Goun, and M. D. Fayer, Chem. Phys. Lett. **374**, 362 (2003).
[88] T. Steinel, J. B. Asbury, J. Zheng, and M. D. Fayer, J. Phys. Chem. A **108**, 10957 (2004).
[89] D. Aherne, V. Tran, and B. J. Schwartz, J. Phys. Chem. B **104**, 5382 (2000).
[90] M. S. Pshenichnikov (private communication).
[91] F. H. Stillinger, Science **267**, 1935 (1995).
[92] T. Steinel, J. B. Asbury, S. A. Corcelli, C. P. Lawrence, J. L. Skinner, and M. D. Fayer, Chem. Phys. Lett. **386**, 295 (2004); J. D. Eaves, J. J. Loparo, C. J. Fecko, S. T. Roberts, A. Tokmakoff, and P. Geissler, Science (to be published).